Pure appl. geophys. 160 (2003) 1273–1313
0033–4553/03/071273–41

Pure and Applied Geophysics

Numerical Modelling of Tsunamis Generated by Hypothetical Landslides in the Strait of Georgia, British Columbia

ALEXANDER B. RABINOVICH,[1,3] RICHARD E. THOMSON,[2] BRIAN D. BORNHOLD,[1] ISAAC V. FINE,[1] and EVGUENI A. KULIKOV[1,3]

Abstract—A modified and corrected version of the viscous slide model of JIANG and LEBLOND (1994) is used to assess the tsunami risk associated with hypothetical underwater slope failures in two coastal areas of British Columbia having potentially unstable sediment deposits: (a) Malaspina Strait, separating the mainland coast and Texada Island in the central Strait of Georgia; and (b) Roberts Bank on the foreslope of the Fraser River Delta in the southern Strait of Georgia. The intent of this study is to demonstrate the capability of the model for tsunami risk assessment and to improve upon previous studies of tsunami risk in the region based on reasonable submarine landslide scenarios. The potential risk from tsunamis associated with slide failures has been examined, but the likelihood of failure events themselves was not considered. For the Malaspina Strait scenarios, simulated tsunamis are generated by failure of a lobe of perched sediment situated on the slope of eastern Texada Island. Failure as a flow slide of the estimated 1,250,000 m^3 of sediment generates wave troughs reaching −4.9 m and trough-to-crest heights of 6 to 8 m along the coast of Texada Island. At Cape Cockburn, on the opposite side of the strait, wave heights of 1.5 to 2.0 m are produced. For Roberts Bank, simulated waves are examined for two separate failure scenarios. The larger slide (Case 1) involves the failure of a sediment lobe with lateral dimensions of 7×3 km^2 and volume of 0.75 km^3 while the smaller slide (Case 2) fails a sediment lobe with dimensions of 4×2.6 km^2 and volume of 0.23 km^3. Computations were made both for high (+3 m) and low (−3 m) tide conditions. For both failure volumes, maximum wave amplitudes (up to 18 m for Case 1 and 8 m for Case 2) occur on the coasts of Mayne and Galiano Islands, opposite the source area. Wave amplitudes are much smaller (1 to 4 m) on the mainland coast because of the reflection of the initial waves from Roberts Bank. Additional numerical experiments were conducted for both regions to estimate the sensitivity of the computed tsunami wave heights to input parameters, such as slide viscosity, bulk density, and slide position.

Key words: Tsunami risk, landslide-generated tsunamis, tsunami prediction, numerical modelling, Strait of Georgia.

[1] International Tsunami Research, Inc., 11321 Chalet Road, Sidney, British Columbia, V8L 5M1, Canada.

[2] Fisheries and Oceans Canada, Institute of Ocean Sciences, 9860 West Saanich Road, Sidney, British Columbia, V8L 4B2, Canada. E-mail: ThomsonR@pac.dfo-mpo.gc.ca

[3] Tsunami Center, P.P. Shirshov Institute of Oceanology, 36 Nakhimovsky Prosp., Moscow, 117851, Russia.

1. Introduction

Submarine landslides, slumps, rock falls, and avalanches can generate significant tsunami waves in coastal areas of the World Ocean. Although landslide-generated tsunamis are decidedly more localized than seismically generated tsunamis, they can produce destructive coastal runup and cause severe damage, especially where the wave energy is trapped by the confines of inlets or semi-enclosed embayments (MURTY, 1977; JIANG and LEBLOND, 1992). Among the best known examples of catastrophic landslide-generated tsunamis are the 1958 Lituya Bay and 1963 Vaiont Valley events. The Lituya Bay event of July 10, 1958 was associated with a rockslide at the head of Lituya Bay, Southeast Alaska (Fig. 1), that caused a giant tsunami that impacted the sides of the inlet to a height of 525 m (MILLER, 1960; MURTY, 1977; LANDER, 1996). The Vaiont Valley event occurred on October 9, 1963 when a massive rock slide fell 175 m into a reservoir in the Vaiont Valley, North Italy, creating a wave that destroyed a town and killed approximately 3000 people (WIEGEL *et al.*, 1970; MURTY, 1977).

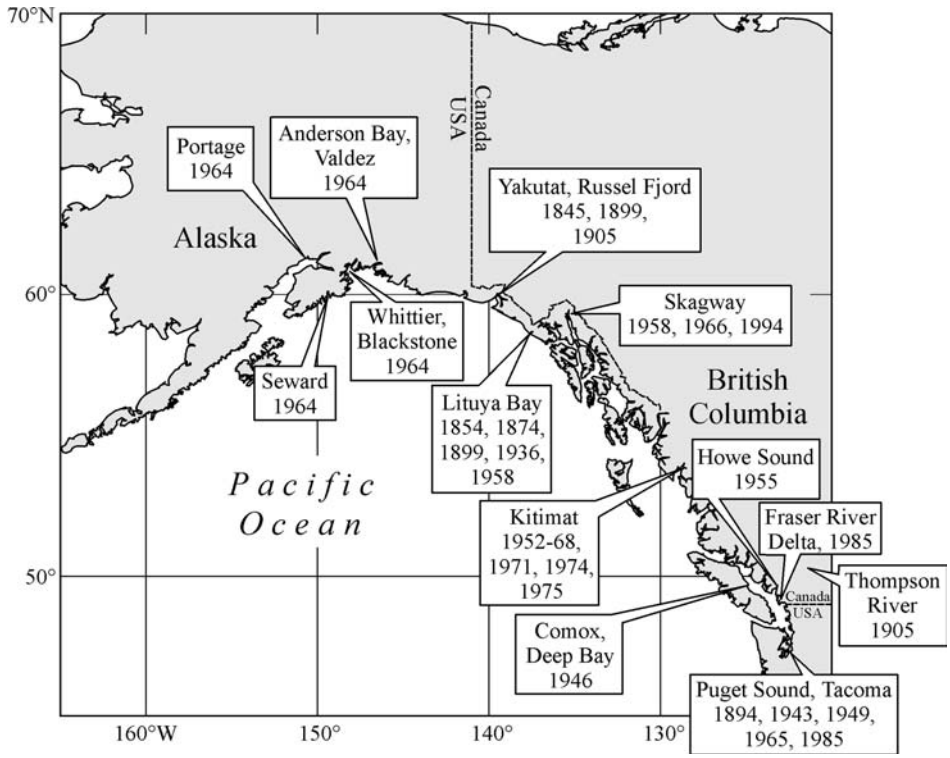

Figure 1
Locations of known submarine landslides and landslide-generated tsunamis along the coasts of Alaska, British Columbia, and Washington.

Although studies of landslide-generated tsunamis have a long history, events themselves are generally considered to be relatively rare. The greatly enhanced interest in this problem over the past few years can be linked to two main causes: (1) Recent destructive earthquake-generated tsunamis in Papua New Guinea, Indonesia, and Turkey; and (2) the well-documented dock failure in Skagway, Alaska. The July 17, 1998, Papua New Guinea (PNG) tsunami, one of the most catastrophic tsunami in the 20th century (about 2300 casualties), appears to have been initiated not by the comparatively modest earthquake of $M_s = 6.9-7.3$, but by a local landslide triggered by the earthquake (TAPPIN *et al.*, 1998; HEINRICH *et al.*, 2000; IMAMURA *et al.,* 2001). Tsunami waves with heights reaching 26 m associated with the 1992 Flores Island Earthquake ($M_s = 7.5$) in Indonesia were apparently induced by local submarine landslides (IMAMURA and GICA, 1996). Local submarine sliding and slumping also contributed to formation of destructive tsunami waves during the 1999 Kocaeli Earthquake, Turkey (ALTINOK *et al.*, 1999). All three events demonstrated that submarine slides play a substantially more important role in tsunami generation than previously thought. It is very likely that many of the so-called "tsunami-earthquakes" (KANAMORI, 1972) – earthquakes that produce considerably stronger tsunamis than would be expected from their magnitudes – were accompanied by submarine landslides which then became local sources of abnormal waves (cf., IWASAKI *et al.*, 1996).

The catastrophic event of November 3, 1994, in Skagway Harbor, Southeast Alaska (Fig. 1) began with the collapse of the Pacific and Arctic Railway and Navigation Company (PARN) Dock and led to a series of large amplitude waves estimated by eyewitnesses to have heights of 5–6 m in the harbor and 9–11 m at the shoreline (LANDER, 1996; KULIKOV *et al.*, 1996). The landslide and associated tsunami claimed the life of one worker and caused an estimated $21 million damage (RAICHLEN *et al.*, 1996). This event initiated intensive scientific discussion. Whereas some authors (KULIKOV *et al.*, 1996; RAICHLEN *et al.*, 1996; CORNFORTH and LOWELL, 1996; RABINOVICH *et al.*, 1999) concluded that the Skagway tsunami was caused by the collapse of the PARN Dock and subsequent landslide, other authors (cf., KOWALIK, 1997) contended that the PARN Dock collapse was initiated by incoming tsunami waves generated by a massive submarine slide in the adjoining basin (Taiya Inlet). A thorough investigation of this case eventually led to greater understanding of slide/wave interaction and to substantial improvement in the numerical modelling of landslide generated tsunamis (see THOMSON *et al.*, 2001 for a detailed description of this case and associated discussion). One of the lessons arising from the Skagway event was the necessity for a thorough examination and modelling of possible submarine sliding/slumping and slide-generated tsunamis in areas of new construction, especially those located in regions of moderate to large tidal ranges and in the vicinity of unstable sediment accumulations.

Coastal and submarine landslides typically have horizontal scales ranging from a few hundred to a few thousand metres. Some large continental slope slides or shelf

glacier falls, such as the Storrega Slides which occurred on the Norwegian continental slope during the Late Quaternary (cf., JANSEN *et al.*, 1987; HARBITZ, 1992), have scales of 20–30 km; however they remain much smaller than scales typical of seismic sources. Because of their localised nature, landslides and associated tsunamis may go undetected (HAMILTON and WIGEN, 1987; LANDER, 1996). At the same time, it is common for landslides to occur regularly at specific sites. For example, field surveys following the 1958 Lituya Bay tsunami indicated that landslide generated tsunamis occurred at this bay in 1853–54 (120 m), 1874 (24 m), 1899 (60 m), and 1936 (150 m) (MILLER, 1960). Similarly, a thorough investigation after the destructive landslide tsunami of April 27, 1975, in Kitimat Arm, British Columbia (Fig. 1), demonstrated that such events had repeatedly taken place in this fjord, in particular in 1952–1968, 1971, and 1974 (MURTY, 1979; PRIOR *et al.,* 1981; JOHNS *et al.*, 1986). Other sites of repeated landslide-generated tsunamis are Yakutat, Russell Fjord, Skagway Harbor (all located in Southeast Alaska), and Puget Sound, Wasington State (LANDER, 1996; CHILLARIGE *et al.*, 1997a; PALMER, 1999) (Fig. 1).

Underwater slopes in fjords and inlets commonly attain a delicate equilibrium with the long-term ambient marine conditions associated with wave, current and tidal regimes, and the rate and character of sedimentation. This stability can be disrupted, leading to failure, by events or conditions that depart significantly from ambient conditions. Landslides, slumps and rock falls are often the secondary effects of earthquakes. The 1958 Lituya Bay rockslide and tsunami, as well as a similar event in 1899, were triggered by strong earthquakes (MILLER, 1960; LANDER, 1996). Submarine landslides that accompanied the 1964 ''Good Friday'' Alaskan earthquake generated wave amplitudes of several tens of metres in certain locations on the Alaska coast (Fig. 1) (LANDER, 1996; PALMER, 1999). The British Columbia Earthquake of 23 June, 1946 ($M = 7.3$) produced many hundreds of local landslides and slumps along the coast of Vancouver Island and most of them generated tsunami waves (ROGERS and HASEGAWA, 1978; ROGERS, 1980). The only death associated with this event was caused when a slump-generated tsunami wave overturned a small boat (ROGERS, 1980).

In many cases, damaging submarine landslides are produced by local processes in the absence of seismic events (EVANS, 2001). In particular, the 1854, 1874, and 1936 Lituya Bay tsunamis and the 1952–1975 Kitimat slides and tsunamis occurred during seismically quiet periods. The 1975 Kitimat Arm failure and tsunami occurred at an extreme low tide and were coincident with coastal construction activity (PRIOR *et al.*, 1984; JOHNS *et al.*, 1985; KULIKOV *et al.*, 1998). Similarly, the 1966 and 1994 Skagway Harbor events coincided with anomalously low tides (see CORNFORTH and LOWELL, 1996; KULIKOV *et al.*, 1998; THOMSON *et al.*, 2001). The same situation existed for the destructive 1894 Tacoma landslide and slide-generated tsunami (H. MOFJELD, Pers. Comm., 1999). Sudden deposition of large sediment loads, especially in deltaic areas during flooding, erosion of the base of the slope, or construction-related loads and activity, as well as meteorological factors such as

rainfall, strong winds, and atmospheric pressure change, are common triggers of subaerial slope failures in coastal zones (cf., REN *et al*., 1996).

Landslide-induced tsunamis have been observed in many Norwegian fjords (BJERRUM, 1971; KARLSRUD and EDGERS, 1980), along the coast of Zeeland, the Netherlands (SILVIS and DE GROOT, 1995; STOUTJESDIJK *et al*., 1997), and the coast of The Levant, Israel (MILOH and STRIEM, 1978), in Yanahuin Lake, Peru, and in Shimabara Bay, Japan (HEINRICH, 1992). However, it is in the inlets and narrow straits of the Pacific Coast of North America (e.g., Lituya Bay, Yakutat, Russel Fjord, Skagway Harbor, Kitimat Arm, Puget Sound) that landslide-generated tsunamis occur most frequently and are accompanied by the largest runup (SOLOVIEV and GO, 1975; LANDER, 1996; PALMER, 1999; EVANS, 2001). For example, in August 1905, a large landslide took place on the right bank of the Thompson River at Spences Bridge in southwestern British Columbia. The landslide generated a displacement wave in the river that ran up the opposite valley wall to a height of 22.5 m, destroyed many buildings in the settlement and killed 15 people (EVANS, 2001). Other locations in British Columbia where landslides have been reported include Howe Sound (TERZAGHI, 1956) and the Fraser River delta region (HAMILTON and WIGEN, 1987; MCKENNA and LUTERNAUER, 1987; MCKENNA *et al*., 1992) (Fig. 1). In general, studies in the coastal areas of Alaska, British Columbia, Washington, Oregon, and California indicate high instability of deltaic and nearshore sediments (PRIOR *et al.,* 1981, 1984; JOHNS *et al.,* 1986). Huge accumulations of unstable sediments deposited in deltas of North American rivers, such as the Fraser, Skeena, and Nisqually, are particularly dangerous (F. STEPHENSON and M. BLACKFORD, Pers. Comm., 2000). Construction sites, buildings, and submarine cables in these areas are at significant risk to direct damage from subaerial and submarine landslides. In these areas, tsunamis generated by the failure events probably pose an even greater threat in terms of damage and loss of life than tsunamis generated by earthquakes. In this respect, it is important to define areas of high landslide risk (especially in new construction zones) and to provide appropriate computations of possible landslide motions and associated tsunamis.

There are several studies of tsunami risk for the Pacific Coast of British Columbia (cf., HEBENSTREIT and MURTY, 1989; NG *et al*., 1990; DUNBAR *et al*., 1991), including the inner coastal region of Juan de Fuca Strait and the Strait of Georgia (cf., MURTY and HEBENSTREIT, 1989; NG *et al*., 1990). However, all these studies are based on numerical simulation of seismically-generated tsunamis caused by distant or local earthquakes in the Pacific Ocean. Very little attention has been paid to the potential risk to these coasts from locally generated landslide-tsunamis (see, for example, the review by CLAGUE, 2001), despite the fact that this type of tsunami is the major threat to this region. DUNBAR and HARPER (1993) is probably the only attempt to estimate the potential threat of slide-generated tsunamis. One of the main purposes of the present study is to fill this gap using modern numerical modelling approaches to estimate tsunami risk for specific coastal areas. As noted by SILVIS and

DE GROOT (1995), *"If the possibility of a flow slide cannot be ruled out, it is necessary to estimate the damage that may occur as a consequence."*

This paper focuses on two localised areas having potential risk of possible underwater slope failure: (a) Malaspina Strait, separating the mainland coast from Texada Island; and (b) Roberts Bank on the southern Fraser River delta, southern Strait of Georgia (Fig. 2). Findings demonstrate the ability of the improved viscous slide model to provide realistic estimates of risk from landslide-generated tsunamis for these two slide scenarios. Three factors sparked our interest in these areas: (1) The

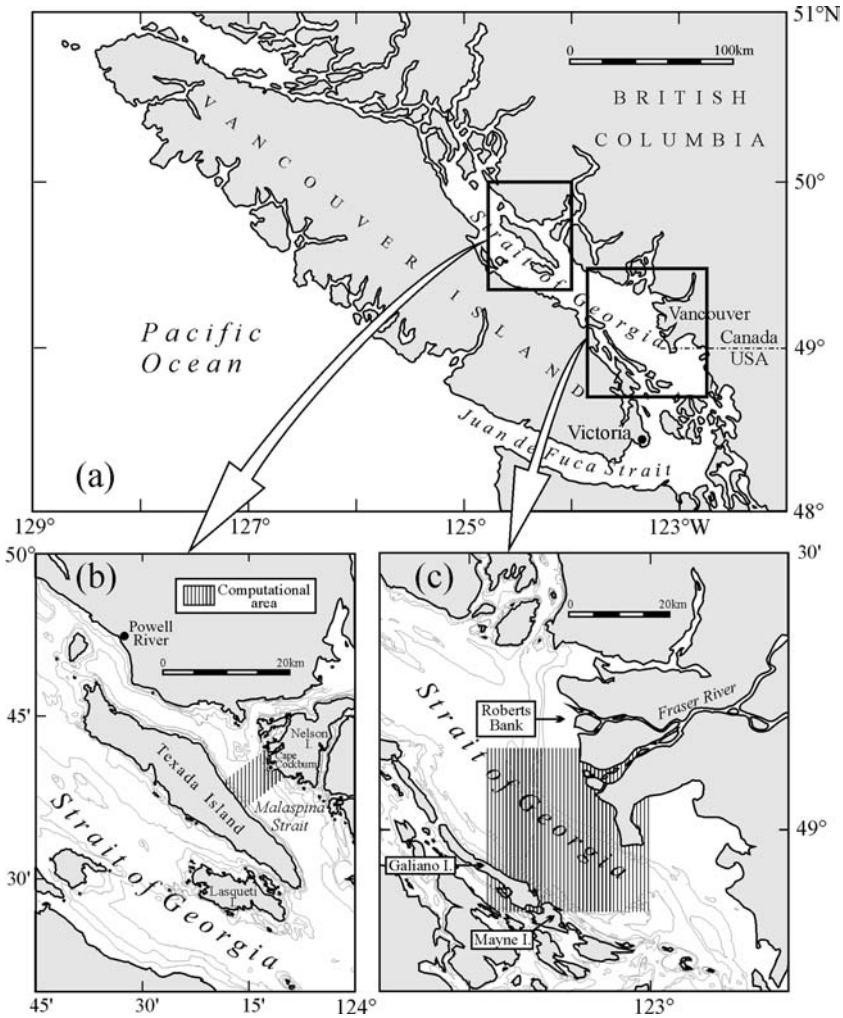

Figure 2
Map of southern British Columbia (a) showing the computational domains (shaded) for Malaspina Strait (b), and the southern part of the Strait of Georgia (c).

large volumes of unconsolidated sediments accumulated in the regions; (2) the possible risk of instability under earthquake loading; and (3) the presence of significant coastal infrastructure, including ferry terminals, port facilities, and electrical transmission cables.

The intent of this study is to demonstrate the application of "state-of-the-art" landslide-tsunami models using various assumptions related to different types and volumes of landslides, not to assess the likelihood of the failure events themselves. *Because of the many uncertainties with respect to sediment physical properties in these areas, the results presented in this paper should be viewed as very preliminary estimations of actual tsunami magnitudes*. We have attempted to present geologically and geotechnically reasonable scenarios based on what is known about the sediments in the area and the seabed morphology. We have also attempted to test a range of likely values for physical properties (e.g., viscosity and friction factors) in the absence of actual data at one of the sites (Texada Island) where direct sampling of the sediments at the site was not permitted because of existing seafloor facilities. This study provides an approach for more detailed studies in this, or other, coastal zones potentially affected by landslides or slumps to determine more rigorously the tsunami risk. We have assumed a single rotational or translational failure of the entire sediment mass. In that way, we develop "worst case scenario." A retrogressive failure would result in lower tsunami amplitudes and a more complex resultant tsunami wavefield. In both instances, insufficient regional geotechnical data were available and the results of these models, thus, should not be used in hazard assessment until further data can be integrated into the models.

Our study makes use of the three-dimensional shallow-water numerical model for viscous landslides (with full slide-wave interactions) developed by JIANG and LEBLOND (1992, 1994) and modified and improved by FINE *et al*. (1998). Customized versions of this model were used to examine the landslide-tsunami event of November 3, 1994, in Skagway Harbor (RABINOVICH *et al*., 1999; THOMSON *et al*., 2001), the 1999 PNG tsunami (HEINRICH *et al.,* 2000; TITOV and GONZÁLEZ, 2001; IMAMURA *et al*., 2001) and the tsunami caused by the slumping of the Nice harbor extension (1979) (ASSIER-RZADKIEWICZ *et al*., 2000).

The paper is organised as follows. Section 2 presents some general ideas on estimating tsunami risk associated with submarine landslides. The numerical model used for the computations is described in Section 3. A short description of the geomorphology of the area of Malaspina Strait, estimates of the unstable sediment body, and results of numerical modelling of the corresponding slide-generated tsunami, are presented in Section 4. Descriptions of the Roberts Bank and Fraser River delta regions, and the results of the respective modelling of tsunami waves for the region of the South Strait of Georgia, are given in Section 5. Sections 6 and 7 present a discussion and summary of the results.

2. Estimation of Impact of Landslide-generated Tsunamis

Long-term tsunami prediction in coastal regions (tsunami-zoning) is a key problem for hazard mitigation and long-term planning (BERNARD, 1998; MOFJELD *et al.*, 1999), including planning for new construction in a coastal zone and for estimating tsunami risk and generating inundation maps for all vulnerable communities (*Planning for Risk*, 1988). Tsunami run-up heights vary significantly throughout neighbouring areas. Thus, the main purposes of long-term tsunami-prediction are to estimate general tsunami risk, to provide local tsunami-zoning (examination of resonant properties of local topography and estimation of possible wave heights along the coast), and to construct inundation maps for the community. The precise estimation of possible tsunami wave heights along the coast is of prime importance. Tsunami wave overestimation greatly increases construction costs, while underestimation significantly increases the risk of destruction including death (RABINOVICH and SHEVCHENKO, 1990). That is why the choice of an adequate model is so important.

There are two different approaches for estimating tsunami risk (*Planning for Risk*, 1988; MOFJELD *et al.*, 1999). One is based on *historical precedents*; i.e., on analysis of tsunami runup observed at a specific site in the past and application of methods of extreme statistics (cf., GO *et al.*, 1985; RABINOVICH and SHEVCHENKO, 1990). The other method is based on numerical modelling of historical or scenario earthquakes and associated tsunamis (cf., HEBENSTREIT and MURTY, 1989; MURTY and HEBENSTREIT, 1989; NG *et al.*, 1990; DUNBAR *et al.*, 1991). An optimum approach is to combine these two methods; i.e., to use observational runup data to verify the numerical model, and to use numerical simulation to extend the observational results. Unfortunately, for most communities, very few or no data exist. This is especially true for new construction areas. For these areas, numerical models (carefully verified with existing data where possible) are the only means by which to obtain estimates of tsunami risk (BERNARD, 1998). Tsunami risk predictions based on numerical simulation of potential tsunamis for existing coastal regions have become an important branch of modern coastal engineering (cf., MOFJELD *et al.*, 1999).

Long-term prediction of landslide-generated tsunamis has a number of specific features:

1. Numerical simulation of earthquake-generated tsunamis normally is based on historical seismic parameters (source characteristics) or on parameters of *hypothetical* earthquakes. For constructing a model of slide-generated tsunamis it is possible to use actual parameters of the unstable sediment body estimated by geotechnical or geophysical methods.
2. Short-time tsunami prediction (tsunami-warning) – which is so important for open ocean tsunamis – has little application to landslide-generated tsunamis because normally the time interval between the event (landslide, slump, or rock

fall) and tsunami waves affecting coastal areas is negligible. For example, during the 1994 Skagway event tsunami waves propagated across to the opposite site of the harbour and destroyed the Ferry Terminal located there in about 20 s after the collapse of the PARN Dock (RAICHLEN *et al.*, 1996; THOMSON *et al.*, 2001). That is why long-term prediction of potential slide-generated tsunamis is especially important.

3. Based on present capabilities, it is not possible to release the accumulated energy of a pending earthquake in order to prevent associated catastrophic tsunamis. Ignoring the liability issue, it may be possible in specific cases to incrementally trigger subaerial or submarine sediment slides (in the same manner as for avalanches) to prevent sediment from accumulating in dangerous amounts and generating significant tsunamis. Using numerical modelling, it is straightforward to consider various scenarios and define the corresponding "triggering" strategy.
4. Seismically-generated ("classic") tsunamis are natural phenomena which occur independently of human activity. In contrast, landslide-generated tsunamis are often the direct result of construction activity in coastal areas (BJERRUM, 1971). Large-scale slides in 1983 at the Nerlerk site, in the Canadian Beaufort Sea, during the construction of a hydraulically placed subsea sand berms are a typical example (SLADEN *et al.*, 1985). Another well known example is the 1979 Nice slide-generated tsunami formed when a part of a new building harbour site slumped into the Mediterranean Sea, producing significant waves and causing several casualties (ASSIER-RZADKIEWICZ *et al.*, 2000).

3. Governing Equations and Model Description

Most geotechnical information for land and marine slides, slumps, avalanches, and rock falls indicate that the commonly used rigid-body approximation of a slide is too simplistic and that the viscous fluid model better describes these processes (cf., ANDRESEN and BJERRUM, 1967; SLADEN *et al.*, 1985; SILVIS and DE GROOT, 1995). For this reason, the viscous fluid slide model, first rigorously formulated by JIANG and LEBLOND (1992, 1994), is now widely used to simulate catastrophic tsunamis arising from submarine landslides. Examples include Nice, France (1979) (ASSIER-RZADKIEWICZ *et al.*, 2000), Skagway (1994) (FINE *et al.,* 1998; RABINOVICH *et al.,* 1999; THOMSON *et al.,* 2001), and PNG (1999) (HEINRICH *et al.,* 2000; TITOV and GONZÁLEZ, 2001; IMAMURA *et al.*, 2001). In all of the above events, the viscous model gives reasonable agreement with the existing empirical data. The consistency between the observed tsunami waves and numerical simulations of these waves using the viscous slide model implies that this is the preferred model for determining landslide-generated tsunami risk along the coast.

The present study is based on the three-dimensional, viscous landslide model proposed by JIANG and LEBLOND (1994). This nonlinear shallow-water (NSW)

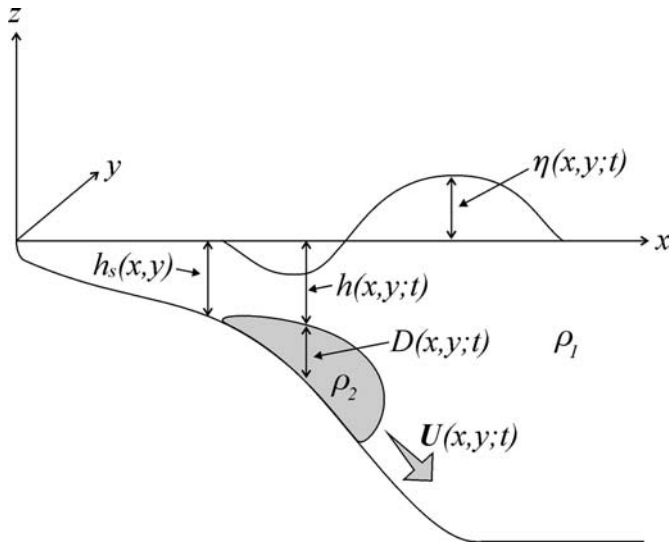

Figure 3
Schematic of a submarine slide and associated surface waves for the viscous slide model.

model gives a reliable description of the slide dynamics and associated surface waves (JOHNSON, 1970; JIANG and LEBLOND, 1992). We have generalised the model to include the actual bottom topography and have corrected a few minor errors in the governing equations in the original publications (see FINE *et al.*, 1998, for details).

Here, the long-wave (hydrostatic) approximation is used for both the surface waves and the slide. This implies that the characteristic length scale of the water waves is much greater than the water depth and that the slide thickness is much less than the slide width and length. Time scales are short compared to a pendulum day, so that Coriolis forces can be neglected. A conceptual model for the slide and associated surface waves is presented in Figure 3. We use standard Cartesian coordinates, x, y, z, with z positive upward. The upper layer consists of seawater with density ρ_1, surface elevation $\eta(x, y; t)$, and horizontal velocity $\mathbf{u}$ with x, y components u, v; t is time. The lower layer consists of sediments of density ρ_2, kinematic viscosity ν, and horizontal velocity $\mathbf{U}$ with components U and V. Both the slope and the slide have small slant angles, so that the motion is essentially horizontal. The slide is bounded by an upper surface $z = -h(x, y; t)$, the seabed is designated by $z = -h_s(x, y)$, and the thickness of the slide is $D(x, y; t) = h_s(x, y) - h(x, y; t)$.

3.1 Viscous Slide Formulation

The main assumptions for the viscous model are:

(1) The slide is an incompressible, isotropic viscous fluid, and seawater is an incompressible inviscid fluid;

(2) The density difference between flowslide and seawater is large, viz. $(\rho_2 - \rho_1) \geq 0.2$ g·cm^{-3} (JIANG and LEBLOND, 1994).
(3) The slide is characterised by laminar, quasi-steady viscous flow. For a finite mass of sediment released on a slope, there will be two distinct flow regimes; inertial and viscous (SIMPSON, 1987). We assume that the viscous regime is rapidly reached after any failure.
(4) Mixing at the water-mud interface is negligible, whereby the slide material is not significantly diluted while flowing downslope.

The main reason for using the viscous model and applying these assumptions is the availability of direct observational data on submarine slides in the Strait of Georgia. Field investigations and offshore geotechnical and geomorphological research show that slides in this region are largely liquefaction flows (CHRISTIAN *et al.*, 1997a,b; CHILLARIGE *et al.*, 1997a,b). The physical background of assumptions (1)–(4) is thoroughly discussed by JIANG and LEBLOND (1992, 1994).

At the seabed, the tangential velocity of the slide is set to zero, while at the upper surface of the slide the normal gradient in tangential velocity is set to zero. At steady state, horizontal velocities in the slide will then have a parabolic profile (JIANG and LEBLOND, 1992, 1994):

$$\mathbf{U}_m(x,y,z,t) = \mathbf{U}(x,y,t)(\xi - \xi^2) \ , \tag{1}$$

where

$$\xi = (z + h_s)/D \tag{2}$$

is a normalised depth.

Conservation of mass and momentum for a viscous slide have the form (FINE *et al.*, 1998):

$$\frac{\partial D}{\partial t} + \frac{2}{3}(\vec{\nabla} \cdot D\mathbf{U}) = 0 \ ; \tag{3}$$

$$\frac{2}{3}\frac{\partial \mathbf{U}}{\partial t} - \frac{2}{15}\frac{\mathbf{U}}{D}\frac{\partial D}{\partial t} + \frac{8}{15}(\mathbf{U} \cdot \vec{\nabla})\mathbf{U} = -\frac{g}{\rho_2}\left[(\rho_2 - \rho_1)\vec{\nabla}(D - h_s) + \rho_1 \vec{\nabla}\eta\right] - \frac{2\nu\mathbf{U}}{D^2} \ , \tag{4}$$

subject to the condition of no slide transport through the coastal boundary, G, and the assumption that the slide does not cross the outer (open) boundary, Γ.

3.2. Surface Wave Formulation

The upper layer of the model is governed by the nonlinear shallow water equations:

$$\frac{\partial(h + \eta)}{\partial t} + [\vec{\nabla} \cdot (h + \eta)\mathbf{u}] = 0 \ ; \tag{5}$$

$$\frac{\partial \mathbf{u}}{\partial t} + (\mathbf{u} \cdot \vec{\nabla})\mathbf{u} = -g\vec{\nabla}\eta \ . \tag{6}$$

In effect, the slide generates water waves through the continuity equation (5) only. The waves then propagate within the restrictions imposed by the boundary conditions and the nonlinear momentum equation (6).

At the open boundary, Γ, we have used the one-dimensional radiation condition for outgoing waves:

$$u_n = \eta\sqrt{\frac{g}{h}} \ , \tag{7}$$

where u_n is the velocity component normal to Γ. At the shore, G, we assume a vertical wall, so that

$$u_n = 0 \quad \text{on } G \ . \tag{8}$$

3.3 Model Approach

An explicit finite-difference method was used to solve equations (3)–(4) for the viscous slide and (5)–(6) for the waves, with boundary conditions (7), (8). We applied a "staggered leap-frog scheme" in space and time (IMAMURA, 1996). An upstream approximation for the advective terms in the momentum equations was used to suppress numerical instability (see ROACHE, 1976, for details). To avoid generation of erroneous small-scale oscillations, the time step (Δt) was chosen to be 1/3 of the value required for the Courant stability condition. Since the slide is initially at rest, all velocity components and the sea-surface elevation are set to zero at $t = 0$.

3.4 Model Verification

Verification of the viscous model included several phases:

(1) Comparison with a rigid-body model

Comparison of our numerical results with analytical results for a rigid-body model (cf., PELINOVSKY and POPLAVSKY, 1996) are in reasonably close agreement, with the viscous model generating smaller waves than the rigid-body model. (Analytical solutions for viscous slide models are difficult to obtain so direct comparisons of analytical results for the two types of wave generation models are not readily possible.)

(2) Comparison with JIANG and LEBLOND (1992, 1994)

Because our viscous slide model is based on the same equations JIANG and LEBLOND (1992, 1994) used in their two-dimensional and three-dimensional slide models, we compute slide motions and associated surface waves similar to those reported in the model results. The slight differences between the two models arises from the minor errors in the constant coefficients in the advective terms of the momentum equations of JLB92 and JLB94 (see FINE *et al.*, 1998 and THOMSON *et al.*, 2001 for details). Numerical experiments using our corrected model result in

20-25% differences in computed tsunami heights compared with the JLB92 and JLB94 models.

(3) Numerical simulation of the 1994 Skagway event

The viscous slide model was successfully used to compute tsunami waves generated by the PARN Dock failure and associated slide in Skagway Harbor on November 3, 1994. Because this tsunami was recorded by a NOAA tide gauge in the harbour (KULIKOV *et al.*, 1996; LANDER, 1996), the viscous slide model could be verified against observations. As illustrated in Figure 4, the results of our numerical simulations are in good agreement with the tide gauge record. More specifically, the simulated wave heights for the tide gauge site agree closely with the tide gauge record, the computed 3.0 min period for the fundamental harbor mode is nearly identical to the observed period, and estimates of the Q-factor ($Q \approx 24$) are comparable to observed values ($Q \approx 21$). Computations for other sites also agree well with eyewitness accounts (see RABINOVICH *et al.*, 1999; THOMSON *et al.*, 2001 for details).

As mentioned in the Introduction, the viscous slide model was also used by others to examine the 1999 Papua New Guinea tsunami (HEINRICH *et al.,* 2000; TITOV and GONZÁLEZ, 2001; IMAMURA *et al.*, 2001) and the 1979 Nice harbour slide-generated

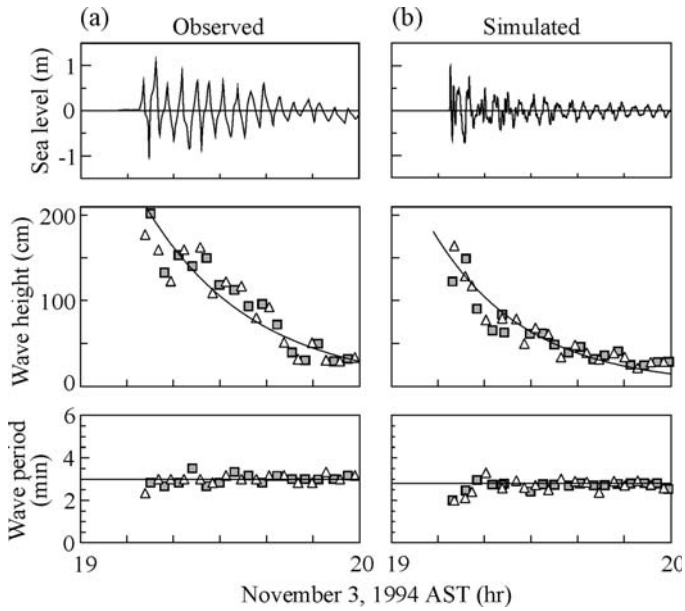

Figure 4

(a) Observed and (b) simulated tsunami records (top panels), variations in wave heights (middle panels), and periods (bottom panels) of the November 3, 1994 Skagway Harbor tsunami. The simulated record was corrected for a 3/4-turn valve opening. Estimated heights and periods are based on successive crests to troughs (triangles) and troughs to crests (squares). The fitted exponential functions approximate the wave height decay. (See RABINOVICH *et al.*, 1999 for details).

tsunami (ASSIER-RZADKIEWICZ *et al.*, 2000). In both cases the model gave reasonable agreement with observations.

4. Malaspina Strait

Malaspina Strait is a narrow (5–10 km), 50-km long channel separating Texada Island in the central Strait of Georgia from the mainland of British Columbia (Fig. 2b). Mid-channel depths throughout the channel range from about 300 to 375 m. The central part of the strait is underlain by a thick (~100 m) sequence of sediments, mostly derived from the Fraser Delta (CURRIE and MOSHER, 1996).

4.1 Submarine slides

The 1946 earthquake in central Vancouver Island, British Columbia produced significant slides and slumps in the coastal areas of Malaspina Strait. Onshore slope failures and clay welting on a beach were observed in the northern part of the strait, and underwater telephone cable lines in the strait were seriously damaged (ROGERS, 1980). Underwater debris flows on the mainland side of northern Malaspina Strait triggered by the 1946 earthquake severed a telephone line to Texada Island.

Geophysical investigations by the Geological Survey of Canada and by others identified a perched sediment mass, divided into two lobes, located along the slope between approximately 30 and 120 m water depth (Figs. 5–6). This unit was identified in initial investigations (high-resolution seismic profiling and sidescan sonar) and was subsequently studied using a remotely operated vehicle (ROV). Extensive video coverage in 1996 of the downslope edge of the unit revealed large (up to several metres) blocks of cohesive sediment, which had collapsed from the front of the unit resulting in a vertical-to-undercut slope in many localities. The lower eroding edge of the unit is everywhere very steep along a scarp-like feature between the 110–120 m isobaths. The failed material has remained just below the scarp on the lower slope (Fig. 2b) as angular blocks of cohesive mud.

The northern lobe is up to 38 m thick and displays internal seaward dips averaging 7.5° (Fig. 6). The unit rests on an underlying slope of approximately 16°, assumed to be bedrock, and extends about 400 m along the slope with a width of approximately 300 m (Fig. 5). While no direct sampling of the sediment was permitted at the site modelled, coring elsewhere in the region (J.V. BARRIE, Pers. Comm., 1997) strongly suggests that the sediment is an overconsolidated Pleistocene glaciomarine mud, possibly underlying the Quadra Sand unit found throughout the Strait of Georgia. Subsequent boreholes on the slope south of the modelled area confirmed this assessment (J.V. BARRIE, Pers. Comm., 2000).

The landslide tsunami modelling presented in the following subsection of this paper considers failure of the northern lobe only. The hypothesized scenario is that

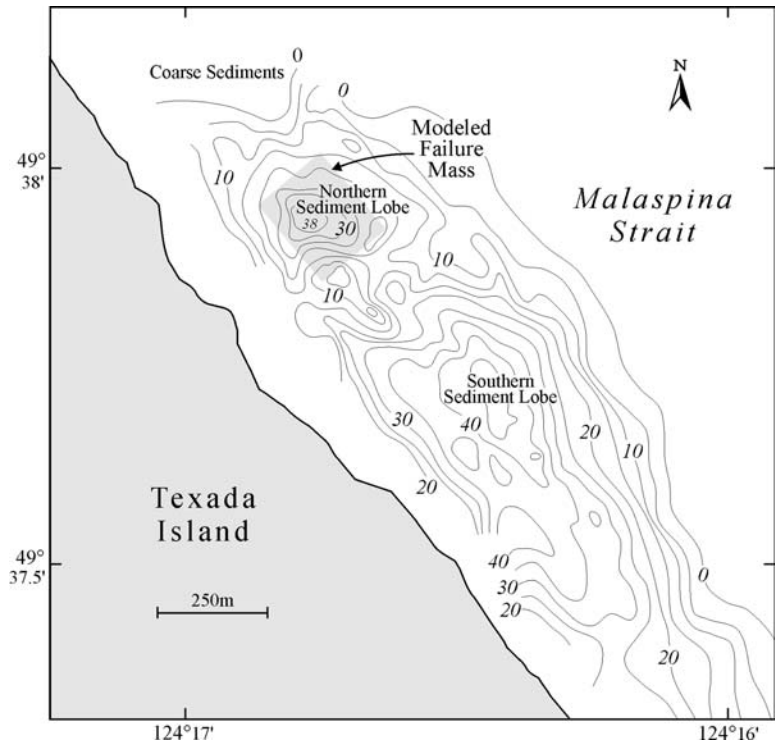

Figure 5
Map of the area off eastern Texada Island showing the distribution of the perched surficial sediment lobes and their thickness on the upper slope. Depth contours are in 5-m increments.

of a severe earthquake causing the entire sediment unit to fail along its steeply dipping basal slope. Because of the lack of geotechnical data, we have examined a broad range of slide input parameters. We have not considered the effects of a simultaneous failure of the much larger southern lobe (more than twice the extent of the northern lobe and more than 45 m thick). For sake of simplicity, we have taken the conservative approach and considered only the northern lobe. Clearly, the tsunami from a combined failure would be much greater than that modelled for the northern lobe alone.

4.2 Numerical Modelling

The numerical model for the Malaspina Strait region has grid dimensions of 365×197 with length steps $\Delta x = \Delta y = 25$ m (Fig. 7). The extent of the submarine landslide on the eastern slope of Texada Island (see Fig. 2b) was based on the known seafloor morphology and sediment deposits (see previous subsection). The initial slide area is rectangular in plan with parabolic cross sections along both axes (as recommended by JIANG and LEBLOND, 1992, 1994) and has the following properties:

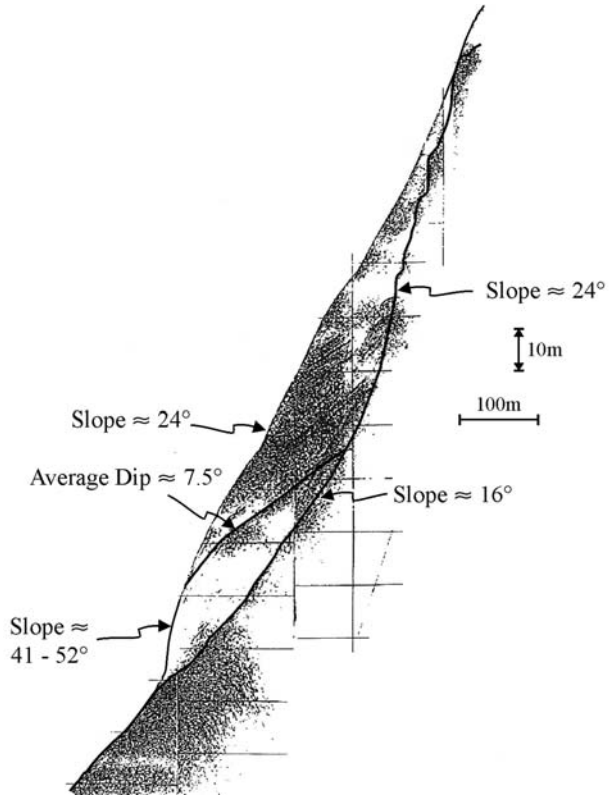

Figure 6
High-resolution seismic profile through the northern sediment lobe, assumed to fail in this investigation, on the eastern slope of Texada Island. Profile reveals the internal structure of the lobe and the steep underlying surface on which the sediment rests.

Volume:	$1,250,000\,\mathrm{m}^3$;
Width:	$200\,\mathrm{m}$;
Mean thickness:	$30\,\mathrm{m}$;
Slide centre coordinates:	$49°37.94'\,\mathrm{N}, 124°16.80'\,\mathrm{W}$;
Mean depth:	$80\,\mathrm{m}$;
Relative position:	$y = 100,\ x = 24$;
Sediment density(ρ_2) :	$2.0\,\mathrm{g}\cdot\mathrm{cm}^{-3}$;
Kinematic viscosity(ν) :	$0.01\,\mathrm{m}^2\cdot\mathrm{s}^{-1}$.

Three sites in the computational area have been chosen as reference points (Fig. 7):
A: (49° 40.380′ N, 124° 12.280′ W) on the eastern shoreline of Texada Island near the slide failure;
B: (49° 40.210′ N, 124° 14.750′ W) in the middle of the channel;
C: (49° 37.865′ N, 124° 16.938′ W) on the western shoreline of Nelson Island, eastern Malaspina Strait.

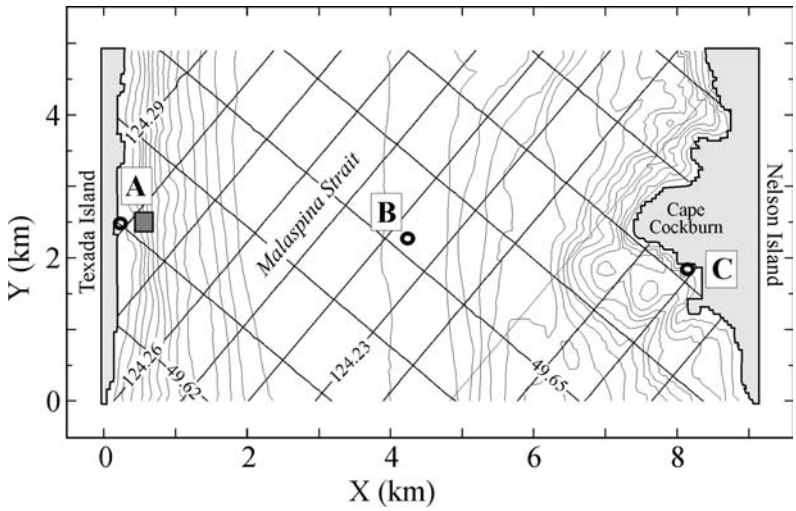

Figure 7
The computational grid used for the Malaspina Strait model, including degrees of latitude and longitude. Wave simulations for sites A, B, and C are provided in the text. Depth contours are in 25-m increments.

The numerical simulations were intended to answer the following questions:

1. What will be the wave heights and periods of the landslide-generated tsunami waves for the chosen computational sites?
2. What will be the extreme runup and rundown distributions along the eastern and western coasts of Malaspina Strait?
3. What would be the maximum speeds associated with the moving slide body?
4. What is the sensitivity of the resulting waves to the chosen initial parameters (density, kinematic viscosity, and slide position)?

Figure 8 presents snapshots of the slide body movement and surface wave propagation. In contrast to rigid slides, which move as consolidated bodies, preserving their size and form, viscous slides spread and flatten as they move downslope (Fig. 8a). Their arcuate shape is a typical feature of moving viscous fluid slides (see, for example, Fig. 3 by JIANG and LEBLOND, 1994). The slide movement is mainly directed normal to the shoreline, spreading cylindrical surface waves ahead of the moving slide. A positive wave (crest) propagates in front of the submarine slide eastward across the strait toward the mainland coast, while a negative wave (trough) moves in the opposite direction (westward) toward Texada Island (Fig. 8b). The occurrence of a shoreward propagating trough is consistent with MILOH and STRIEM (1978) who showed that a recession of the sea occurs when a slide fails downslope (see also JIANG and LEBLOND, 1992). The leading wave transits Malaspina Strait and arrives at Cape Cockburn on Nelson Island about 132 s after the inception of the slide. Following wave refraction on the shelf of Nelson Island and reflection from the coastline, the tsunami waves form a complicated structure of standing oscillations in

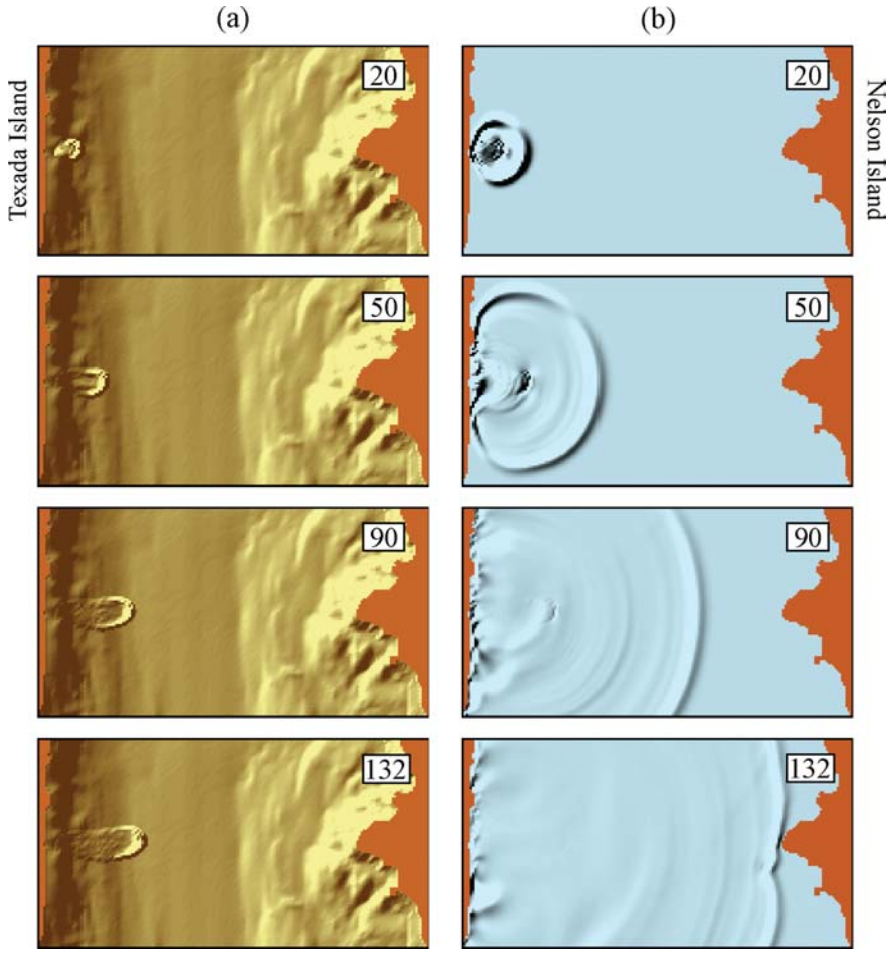

Figure 8
Snapshots of the slide and associated tsunami waves from numerical simulations for times 20, 50, 90, and 132 s after the initial hypothetical slide failure in Malaspina Strait. (a) Viscous slide body; and (b) tsunami.

the strait. Radiation through the open strait boundaries results in rapid decay of these oscillations.

Figure 9 shows simulated wave records (surface water elevations) at sites A, B, and C. Table 1 gives the derived wave characteristics for these sites. Maximum wave heights are observed at Site A, close to the generating area, while minimum heights occur at Site B in the middle of the channel. The first wave is negative at site A and positive at sites B and C. This means that the wave crest precedes the slide in an eastward direction. Wave oscillations attenuate rapidly at sites A and B, apparently because of strong outward radiation of wave energy. In contrast, the oscillations at site C decay slowly, probably due to a trapping effect in this area and the formation

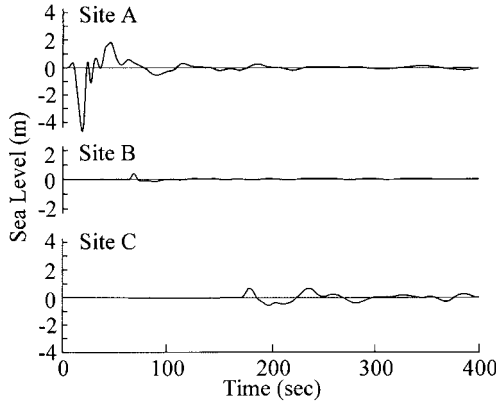

Figure 9
Simulated sea level records at sites A, B, and C (see Fig. 7 for site locations).

Table 1

Wave heights and arrival times for slide-generated tsunamis for various sites in Malaspina Strait

Parameters	Site		
	A	B	C
Leading wave arrival time from start of landslide (s)	6	64	163
		Maximum crest	
Arrival time (s)	50	71	176
Height (m)	1.9	0.5	0.7
		Maximum trough	
Arrival time (s)	24	90	195
Height (m)	−4.8	−0.2	−0.5

of standing oscillations over the shelf. The periods of the simulated wave oscillations shorten with time from 80 to 40 s.

Using the viscous slide model, we estimated maximum trough and crest heights along the western and eastern coasts of the strait (Fig. 10). As our results indicate, maximum wave troughs (up to −5 m) are observed in the vicinity of the source area. Northward and southward from this area, the trough amplitudes decay rapidly. Maximum wave crests are also observed along the western coast, though smaller than troughs (up to +2.7 m) and distributed in a more irregular way. On the opposite (eastern) coast both trough and crest amplitudes are much smaller (about ± 1 m) and less spatially consistent. The much greater variability in wave height along the eastern (Nelson Island) coast in comparison with the western (Texada Island) coast appear to be related to local topographic irregularities of the western coastline.

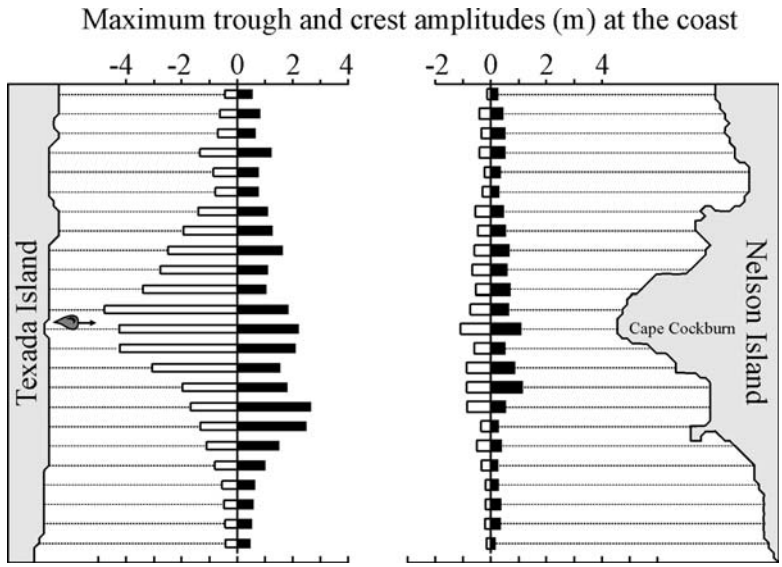

Figure 10
Maximum negative (trough) and positive (crest) amplitudes computed along the western and eastern coasts of Malaspina Strait.

4.3 Sensitivity Analysis

The estimated tsunami wave heights presented in the previous section are based on realistic physical properties for the region obtained from CURRIE and MOSHER (1996), and J.V. BARRIE (Pers. Comm., 1997, 2000, 2001). Despite our confidence that the resulting simulations are representative of wave heights generated by major submarine failures in Malaspina Strait, it is nevertheless important to provide sensitivity tests of the model for a range of sediment and slide-body parameters. In the present study, the sensitivity tests consisted of numerical simulations of extreme wave crest and trough heights (Table 2) for a wide range of slide density ($1.6 \leq \rho_2 \leq 2.2$ g $\cdot$ cm^{-3}), slide kinematic viscosity ($10^{-3} \leq \nu \leq 10^{0}$ m^2 $\cdot$ s^{-1}), and offshore slide position ($600 \leq x \leq 800$ m).

Kinematic viscosity is the least determinate parameter of a slide. Fortunately, the influence of this parameter on tsunami heights is small, with a change in ν from 0.001 to 0.1 m^2 $\cdot$ s^{-1} causing a change in tsunami amplitude of only about 1%. Variations in slide density are more important. For this parameter, a change in density ρ_2 of 0.4 g $\cdot$ cm^{-3} (from 1.6 to 2.0 g $\cdot$ cm^{-3}) results in an increase of simulated tsunami amplitudes of 20%. However, for density variations < 0.1 g$\cdot$cm^{-3}, changes in tsunami wave height are negligible. In contrast, the effects on simulated tsunami waves of changing the initial slide position (x) or the associated mean water depth are significant. This "sensitivity" of tsunami wave height to initial position and depth is especially valid when the source area is situated along

Table 2

Maximum crest and trough heights for three sites in Malaspina Strait computed for various initial viscous slide parameters

Parameters	Sites					
	A		B		C	
	Crest (m)	Trough (m)	Crest (m)	Trough (m)	Crest (m)	Trough (m)
Slide density ($g \cdot cm^{-3}$) (1)						
1.6	1.68	−3.78	0.31	−0.08	0.50	−0.30
1.8	1.82	−4.36	0.40	−0.12	0.63	−0.41
1.9	1.86	−4.58	0.45	−0.13	0.68	−0.47
2.0	1.90	−4.78	0.49	−0.15	0.74	−0.53
2.1	1.93	−4.95	0.53	−0.16	0.78	−0.58
2.2	1.96	−5.11	0.57	−0.18	0.83	−0.63
Kinematic viscosity ($m^2 \cdot s^{-1}$)(2)						
0.001	1.90	−4.78	0.49	−0.15	0.74	−0.51
0.01	1.90	−4.78	0.49	−0.15	0.74	−0.53
0.1	1.92	−4.75	0.48	−0.16	0.71	−0.59
1.0	1.89	−4.59	0.43	−0.20	0.61	−0.55
Slide position (m)(3) Distance/Mean depth						
−100/51	3.48	−8.80	0.57	−0.16	0.89	−0.55
−50/64	2.53	−6.63	0.52	−0.16	0.79	−0.47
0/80	1.90	−4.78	0.49	−0.15	0.74	−0.53
50/98	1.60	−3.57	0.43	−0.16	0.66	−0.53
100/118	1.30	−2.71	0.36	−0.15	0.55	−0.46

(1) Computations are made for different density values for fixed viscosity $v = 0.01\ m^2 \cdot s^{-1}$.
(2) Computations are made for different viscosity values for fixed slide density $\rho_2 = 2.0\ g \cdot cm^{-3}$.
(3) Computations are made for fixed slide density $\rho_2 = 2.0\ g \cdot cm^{-3}$ and viscosity $v = 0.01\ m^2 \cdot s^{-1}$ and various offshore slide positions relative to $x = 600$ m. Corresponding mean depths of the slide body are indicated.

the coast of Texada Island. For example, shifting the source area 100 m closer to the shoreline (i.e. reducing the mean slide water depth by about 30 m) causes an 85% amplification of the generated tsunami waves; shifting the source area 100 m further offshore (from 80 m to 118 m depth) reduces the wave heights by about 70%.

Additional numerical tests have shown that the simulated wave heights are roughly proportional to the volume of the slide body. Thus, slide volume and position (mean depth) are two key parameters determining tsunami wave heights for Malaspina Strait and similar coastal regions. If these two main slide properties are known (as in our case for the northern lobe shown in Figs. 5 and 6), tsunami wave heights may be estimated with relatively high accuracy.

5. Southern Strait of Georgia: Roberts Bank and Fraser River Delta

The Strait of Georgia is a long (222 km) and narrow (28 km) channel separating Vancouver Island from the mainland of British Columbia (Fig. 2). The average depth within the strait is about 155 m. It is linked to the Pacific Ocean via Juan de Fuca Strait and several channels between the San Juan and Gulf Islands. Freshwater discharge into the strait comes mainly from the Fraser River, which empties directly into the basin near Vancouver. The mouth of the Fraser River ajoins the Strait of Georgia along a 37-km delta front from Point Grey to Point Roberts Peninsula. The delta has been adding sediments at high rate and forms deposits 100–200-m thick over glacial deposits. Roberts Bank is the main area of accumulated alluvial deposits. It is located at the entrance of the South Arm of the delta between Sand heads in the north and Point Roberts Peninsula in the south (THOMSON, 1981). *"The marine portion of the delta hosts the busiest ferry terminal in the world at Tsawwassen, the largest coal and containerized shipping facility in Canada, major hydroelectric and communication cable corridors connecting Vancouver Island to the mainland, a large fishing industry, and several ocean damping sites"* (CHRISTIAN *et al.*, 1997b). The large unstable sediment mass (10^9 m^3) identified on the Roberts Bank slope (CHRISTIAN *et al.*, 1997a,b) could potentially result in significant submarine landslides and associated tsunamis and would likely produce severe damage.

5.1 Submarine Landslides

The southern Strait of Georgia has been identified as a region potentially at high risk from submarine landslides (cf., TERZAGHI, 1956; TIFFIN *et al.*, 1971; HAMILTON, and LUTERNAUER, 1983; CHRISTIAN *et al.*, 1995, 1997a,b; CHILLARIGE *et al.*, 1997b). The Fraser River discharges up to 10,000 $m^3 \cdot s^{-1}$ of silt-laden waters into the strait (see Fig. 11) with an annual sediment load of $\approx$17.3 million tonnes (CURRIE and MOSHER, 1996). Unconsolidated sediments deposited off Roberts Bank produce an unstable delta front. The instability of the foreslope on the Fraser River delta has long been known (cf., TERZAGHI, 1956; MATHEWS and SHEPARD, 1962; HAMILTON and LUTERNAUER, 1983). Two very general types of failure may occur in this region: (1) Shallow, retrogressive flow slide failures, and (2) deep-seated large-scale rotational failures (TIFFIN *et al.*, 1971; HAMILTON and WIGEN, 1987; CHRISTIAN *et al.*, 1995). Five known flow slides occurred in the Fraser River delta between 1970 and 1985 (MCKENNA *et al.*, 1992; CHILLARIGE *et al.*, 1997a,b). A failure in July 1985 was documented by MCKENNA and LUTERNAUER (1987) and MCKENNA *et al.* (1992) who assumed that the failure was a "slow retrogressive flow over a period of hours" so that no tsunamis were generated. However, according to HAMILTON and WIGEN (1987) and DUNBAR and HARPER (1993), more rapid (second-type failures) may generate significant tsunamis with amplitudes exceeding several metres. Tsunamis, in combination with high tide and storm surges, could cause coastal flooding in this area of the

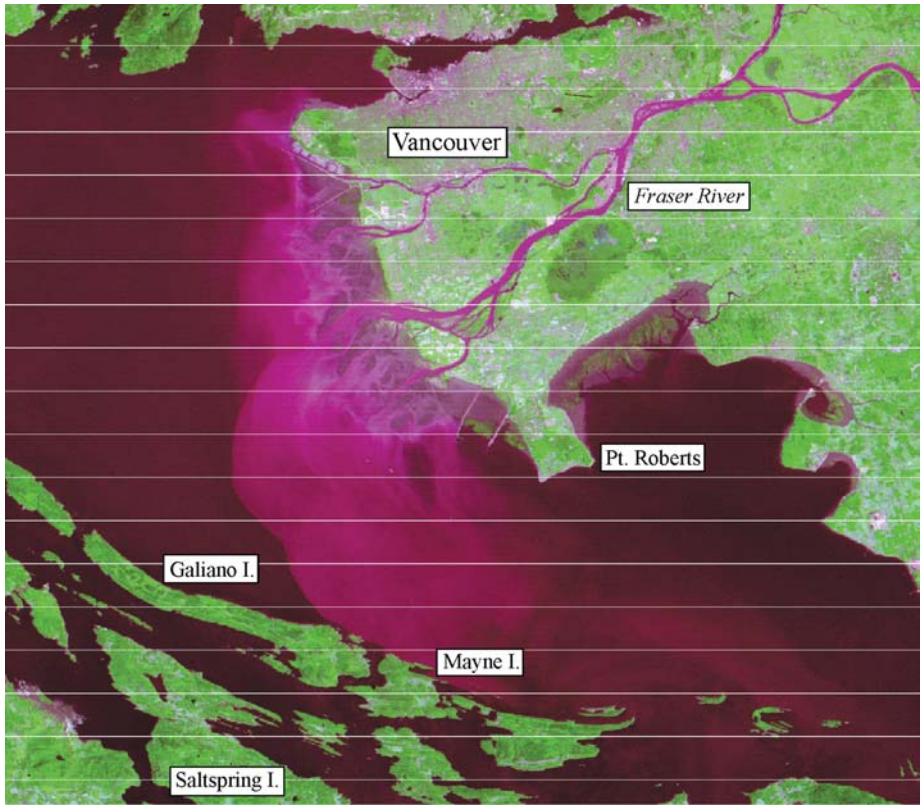

Figure 11
ERTS-1 satellite image of the Fraser River delta and plume on August 12, 1973. Spatial resolution is about 80 m. The colour is infrared composite image showing vegetation as green, clear water as deep violet, and muddy water as light violet. Tide is low, exposing mud flats and eel grass (courtesy of Jim Gower, IOS).

Strait of Georgia, with possible loss of life. As noted by HAMILTON and WIGEN (1987) "*Such a disturbance radiating from Sand Heads in the central Strait of Georgia would easily propagate both up the Strait (NW) to affect urban centres like Nanaimo, Parksville, Comox, Powell River and Campbell River, by reflection into Burrard Inlet and down the Strait (SE) to affect the American San Juan Islands and Puget Sound.*"

An intensive collaborative effort was begun in 1992 to determine geological and geotechnical properties of the offshore portion of the Fraser River delta, to identify seabed instability processes and to map their characteristics (CHRISTIAN *et al.*, 1997a,b). Roberts Bank is one of the main areas of alluvial sediment instability. Much has been written about the potential for submarine slope failures on Roberts Bank, driven by concerns for the security of infrastructure in the area. The western edge of the modern Fraser Delta consists of a broad tidal flat extending about 6 km to the top of the delta front slope at about 9 m depth. The upper delta front is

characterised by slopes of up to 23°, diminishing to 1 to 2° at 300 m depth in the adjacent Strait of Georgia basin. Approximately 100 to 110 m of Holocene silts and sands have accumulated at the edge of the delta platform. These sediments overlie stiff, Pleistocene diamictons and coarse outwash deposits (CHRISTIAN *et al.*, 1995). The depth to the top of the Pleistocene deposits is only about 9 m at the landward end of the BC Ferry Terminal Causeway; Pleistocene deposits make up Point Roberts.

The shallow Holocene delta foreslope deposits consist of channel and turbidite sands interstratified with silts (CHRISTIAN *et al.*, 1995). The bottomset beds over which the delta has prograded are generally finer grained than the foreset beds. In a borehole at the end of the Coal Port, a zone of "stiff silt grading down to sensitive clay, medium to low plasticity, bioturbated" was sampled between about 102 and 109 m depth (CHRISTIAN *et al.*, 1995). These fine-grained marine sediments may also be undergoing leaching by freshwater infiltration through the underlying Pleistocene sediments, leading to formation of sensitive clays. CHRISTIAN *et al.* (1995) consider the possibility of failure of the Roberts Bank area along this horizon of fine-grained bottomset sediments. They have concluded that failure within a basal marine clay layer was responsible for the creation of the Foreslope Hills. For this reason CHRISTIAN *et al.* (1995) urge careful re-evaluation of the engineering characteristics of these basal marine sediments.

HAMILTON and WIGEN (1987) were probably the first to discuss the possibility (and some probable historical precedents) for tsunamis in the southern part of the Strait of Georgia generated by the Foreslope Hills failure in the area of the Fraser River delta. DUNBAR and HARPER (1993) (herein DH93), using a relatively coarse (2 km^2) grid, undertook a preliminary simulation of tsunamis in this area assuming a large delta front slide (from 2.5 to 7.5 km^3) as the source. The DH93 numerical model represented the slide volume as a large number of independent slabs acting under the influence of gravitational acceleration and friction. Their study showed that such slides may induce tsunamis with heights from 1 to 4 m. Our study uses much smaller volumes (from 0.23 to 0.75 km^3), but applies a more realistic numerical model of a viscous slide similar to that used in previous sections to model hypothetical landslide-generated tsunamis in Malaspina Strait. We would like to emphasise that there are no specific geotechnical data which would suggest that, under anticipated earthquake loading, failure would actually occur; we have merely assumed that failure *would occur* and then estimate possible tsunami waves which could be produced by such a failure. More extensive geotechnical studies are required before actual tsunami risk assessment can be carried out.

5.2 Numerical Modelling

Guided by available qualitative borehole information and assessments discussed above, two failure scenarios are postulated for the edge of Roberts Bank: (a) A large

(0.75 km^3) failure occurring at a depth of about 100 m (the zone of postulated sensitive clays), extending 7 km along the delta front between Canoe Passage and the BC Ferry Terminal with a swath width of 3 km; and (b) a smaller (0.23 km^3) failure, also occurring at a depth of 100 m, extending 4 km from Westshore Terminals to the BC Ferry Terminal with a width of 2.6 km (Figs. 2c and 12). The chosen position of the slide failure is very close to that marked Figure 1 of CHRISTIAN *et al.* (1997b). We assume that if leaching to produce sensitive clays were an important condition leading to failure, then the area of Roberts Bank south of Canoe Passage would be more susceptible than the area to the north. In our estimation, any artesian flow would be more intense farther south along the bank (P. MONAHAN, Pers. Comm., 1997). All failures were assumed to be submarine and were modelled for both high-tide and low-tide conditions.

Bathymetric data, including recently acquired multibeam echosounding, were used to define the morphology of the basin. These data were important in determining both the character of the resultant tsunami waves and the extent of the flow slides on the basin floor. The Roberts Bank slide was assumed to have a rectangular bottom boundary at an angle of 28° relative to the computational grid (see Fig. 12), but the thickness of the slide was taken from the actual geomorphic measurements above the uniform slope.

The computational area (Fig. 12) had grid dimensions 309×269 with length steps $\Delta x = \Delta y = 100$ m. The Strait of Georgia is characterised by large tides with tidal amplitudes up to 3 m (F. STEPHENSON, Pers. Comm., 1997). These tides significantly change the geometry of the coastal area in the vicinity of the Fraser River delta. As a consequence, our computations have been made for two different grid areas, corresponding to extreme high water (3 m above sea level) and extreme low water (3 m below mean sea level). The main difference between these areas occurs in the vicinity of Roberts Bank. During high water, the area is under water, during low water, the area is fully drained (Fig. 12). Computer animations were developed for the two cases of sediment failure and for both high and low tides, for a total of 4 simulations.

Figure 13 presents snapshots of the slide body and tsunami wave patterns for Case 1 at high tide for times $t = 1$, 3, 6, and 10 min. The advancing submarine slide and intensification of the southwestward propagating wave crest are clearly evident. The waves cross the strait in about 7 min, reflect from the coasts of Galiano and Mayne islands, and then spread into the open strait. After multiple reflections from both coasts, and scattering from shore irregularities, the waves form a "chaotic" pattern of standing and propagating oscillations (Fig. 13b, at $t = 10$ min). Figure 13 also shows the large extent of the flow slide run-out.

Time series of the simulated tsunami waves have been calculated for six locations shown in Figure 12: (1) The mainland shoreline in the northern part of Roberts Bank; (2) the mid-channel region in the southern Strait of Georgia; (3) the southernmost part of Point Roberts (United States); (4) the shoreline of northeastern

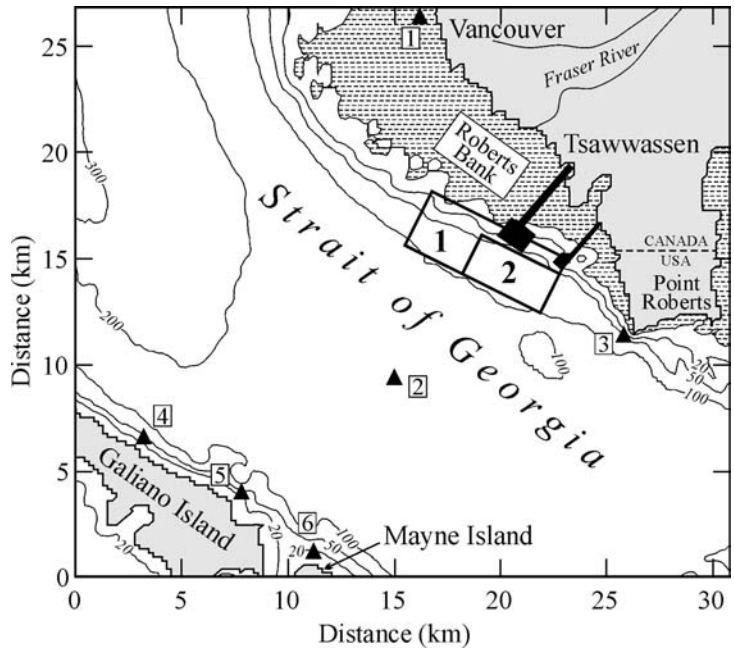

Figure 12
The computational domain used for the southern Strait of Georgia models. Dashed region denotes the area assumed to dry at low tide. Bold numbers refer to the modelled slide-body source areas for Cases 1 and 2. Specific computational sites 1 to 6 are marked.

Galiano Island; (5) the shoreline of southeastern Galiano Island; and (6) the shoreline of northern Mayne Island. The results of the computations are presented in Figure 14 and Tables 3 and 4. For both slide cases, maximum simulated waves were observed at locations 4, 5, and 6; i.e., on the coasts of Mayne and Galiano islands (opposite the source area) and in the middle of the strait (Site 2). For Case 1, positive waves with crest amplitudes of 12.9 m were generated at Mayne Island (Site 6) for low water conditions. For high water conditions, the crest amplitudes were 12.2 m. Negative waves associated with these events had trough amplitudes of -10.4 m for low-tide conditions and -6.4 m for high-tide conditions. On the mainland coast, amplitudes of the tsunami waves were much smaller, apparently because of wave reflection near Roberts Bank. Crest amplitudes for low tide were always somewhat greater (5–10%) than for high tides. Low tide versus high tide differences were much greater for wave troughs, with larger troughs typically observed at low tide (Table 3). For Case 2 (the smaller sediment failure) results were qualitatively similar to Case 1, but all amplitudes were approximately 2–3 times smaller (Table 4).

An important aspect of the modelled tsunami wavefield is that Roberts Bank efficiently reflects the waves and protects the mainland coast (see Fig. 13b). This is why maximum waves are observed opposite the source area, rather than on the

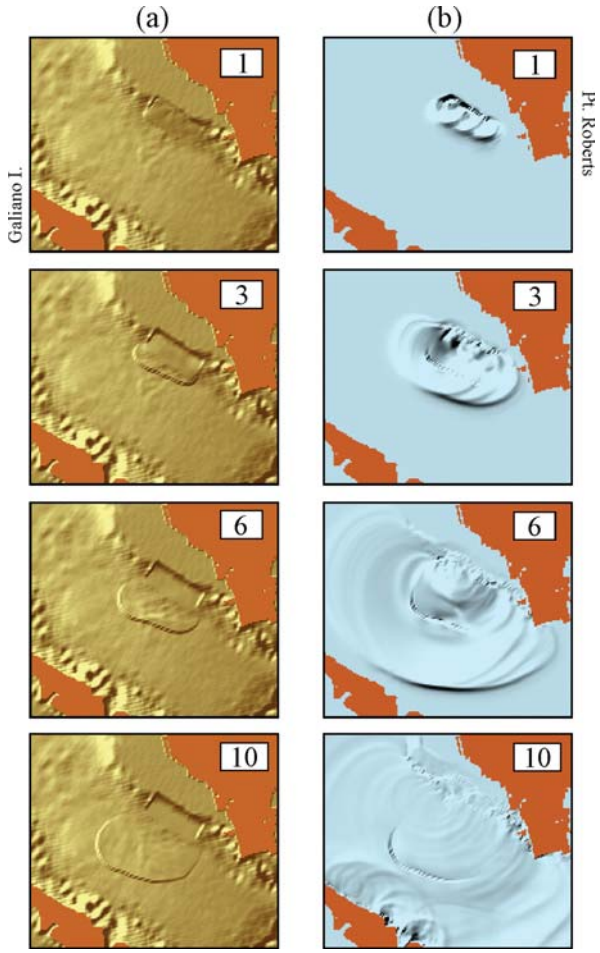

Figure 13
Snapshots of the simulated slide and tsunami fields at 1, 3, 6, and 10 min after the hypothetical slide failure in the vicinity of Roberts Bank for Case 1 at the time of high tide. (a) Movement of the slide body; and (b) propagation of the tsunami waves.

northeastern coast of the strait near the initial failure zone (Figs. 14 and 15). A similar result was obtained for low tide. From this point of view, these results are in contrast with those obtained for Malaspina Strait, where maximum amplitudes of the simulated tsunami waves were observed for the coast located nearest the source area.

As indicated by Figure 14 (see also Tables 3 and 4), the maximum wave heights are associated with the leading tsunami waves produced by the hypothetical Fraser Delta failures. In this respect, our results differ from the modelling results of DUNBAR and HARPER (1993) (DH93 model) who found that the maximum waves occur more than 3 hours after the beginning of the failure in some locations. In addition,

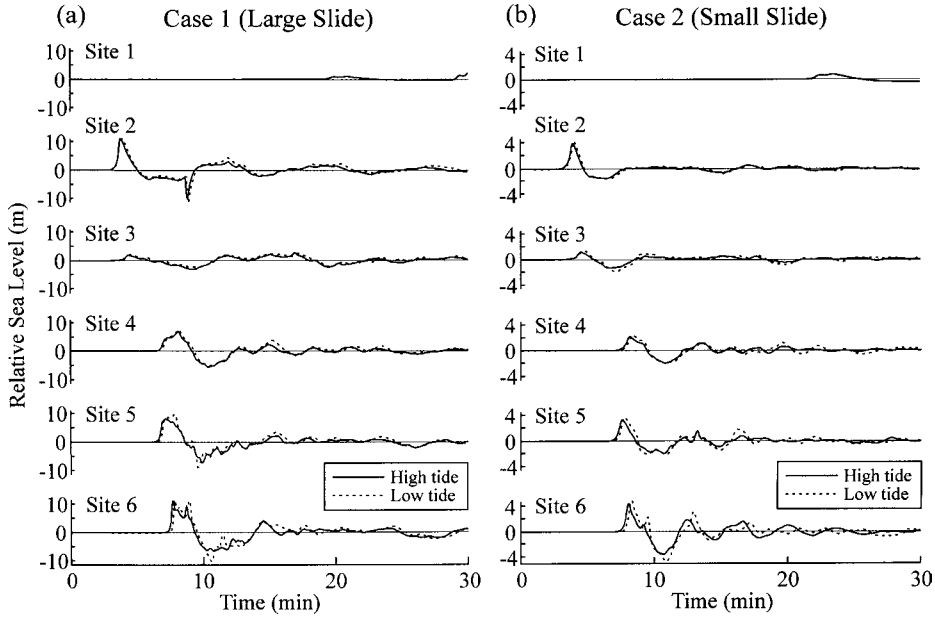

Figure 14
Simulated sea level records at Sites 1 to 6 (see Fig. 11) in the southern Strait of Georgia computed for (a) Case 1; and (b) Case 2. Computations are made for both high and low tide.

Table 3

Timing and amplitude values for simulated landslide-generated tsunamis for sites in the southern Strait of Georgia for Case 1 (large slide with horizontal dimensions 7×3 km^2) computed for high tide (3 m above mean sea, MSL) and low tide (3 m below MSL) (in brackets). NA = not applicable

Parameters	Site					
	1	2	3	4	5	6
Leading wave arrival time (min)	19.0 (NA)	2.8 (2.8)	3.4 (3.5)	6.3 (6.5)	6.2 (6.3)	7.0 (7.2)
			Maximum crest (positive wave)			
Arrival time (min)	30.0 (NA)	3.8 (3.9)	11.3 (17.1)	8.1 (8.2)	7.2 (7.3)	7.7 (7.9)
Amplitude (m)	2.1 (NA)	11.1 (11.9)	2.0 (2.6)	6.9 (7.5)	8.1 (8.8)	12.2 (12.9)
			Maximum trough (negative wave)			
Arrival time (min)	28.5 (NA)	8.9 (8.9)	9.3 (9.2)	10.4 (10.6)	9.9 (10.4)	10.3 (10.6)
Amplitude (m)	−0.4 (NA)	−10.1(−11.2)	−3.1(−2.5)	−5.6(−5.0)	−7.3(−5.3)	−6.4(−10.4)

computed wave heights were much smaller in the DH93 model (from 1 to 4 m) than in the present model, despite the fact that total slide volume used in the DH93 model was about ten times larger (from 2.5 to 7.5 km^3). There are three main reasons for these differences:

Table 4

The same as in Table 3 but for Case 2 (small slide with horizontal dimensions $4 \times 2.6\ km^2$*)*

Parameters	Site					
	1	2	3	4	5	6
Leading wave arrival time (min)	21.5 (NA)	2.9 (2.9)	3.2 (3.3)	7.1 (7.3)	6.6 (6.7)	7.3 (7.1)
			Maximum crest (positive wave)			
Arrival time (min)	23.4 (NA)	3.9 (4.0)	4.6 (4.7)	8.2 (8.4)	7.6 (7.8)	8.3 (8.1)
Amplitude (m)	0.8 (NA)	4.2 (4.3)	1.2 (1.3)	2.1 (2.3)	3.3 (3.6)	4.9 (4.4)
			Maximum trough (negative wave)			
Arrival time (min)	30.0 (NA)	6.4 (6.8)	6.6 (7.2)	10.8 (10.9)	10.7 (9.5)	9.5 (10.7)
Amplitude (m)	−0.4 (NA)	−1.5(−1.5)	−1.3(−1.9)	−2.0(−2.1)	−1.9 (−2.1)	−2.3 (−3.5)

1. The DH93 model simulated the submarine slide as a large number of independent slabs which moved down the slope for about 1 hour, continuously generating water waves. This model has a *distributed* source in time and space. In contrast, we simulated the slide as a *single* viscous body, which is a much more efficient tsunami generator than the retrogressive slide. The largest waves in the single slide case are generated by the initial failure. Our results could, thus, be considered a "worst case" scenario for the volumes assumed.
2. The slide source area in the DH93 model was located in deeper water (between the 50 and 250 m depth contours) than the present model (between the 3 and 100 m depth contours). The efficiency of moving slides as tsunami generators decreases with increasing water depth (see Table 2).
3. We used a more detailed computational grid area (spatial step $\Delta x = \Delta y = 0.1$ km) compared with $\Delta x = \Delta y = 2.0$ km for DH93. High spatial resolution enables us to resolve specific resonance features of the local topography and estimate more accurately the extreme wave heights along the coast.

There are marked variations in wave height from one site to another (Fig. 14), indicating the strong influence of local topography on the heights of tsunami waves. To better examine this effect, and to estimate possible tsunami risk for various coastal sites, we computed maximum trough and crest amplitudes along the southwestern and northeastern coasts of the strait. The respective results for Case 1 (high tide) are shown in Figure 15. The main features of these computations are as follows:

1. Hypothetical tsunami waves generated by our model along the southwestern coast of the strait (Galiano and Mayne islands) are much larger than along the northeastern coast (Tsawwassen); maximum crests are from +4 to +18 m and maximum troughs from −3 to −12 m for the southwestern coast compared to +1.5 to +5 m and −0.2 to −5 m for the northeastern coast.

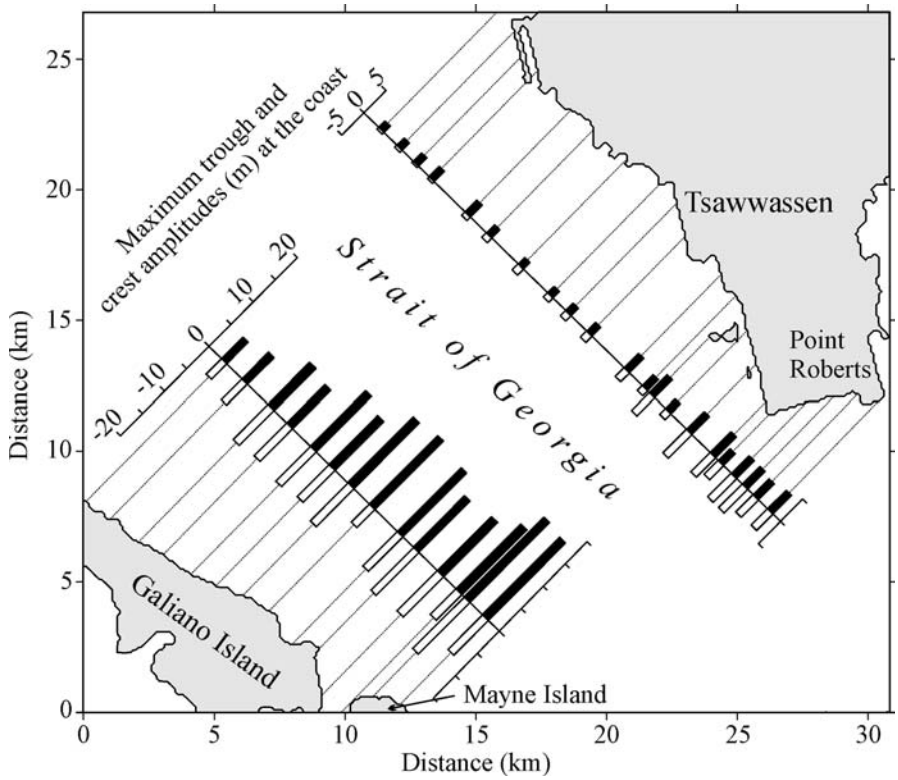

Figure 15
Maximum negative (trough) and positive (crest) wave amplitudes computed along the western and eastern coasts of the southern Strait of Georgia for Case 1 at high tide.

2. For both the southwestern and northeastern coasts of the strait, there is a tendency for a north-to-south increase in wave amplitudes, with minimum computed amplitudes at the northernmost end of Galiano Island and the coast north of Tsawwassen; maximum amplitudes occur on the coasts of Mayne Island and Point Roberts.
3. For both coasts, crest amplitudes are significantly larger than trough amplitudes, the exception being the coast of Point Roberts where they are approximately equal (4 to 5 m).
4. Complicated coastal geometry and seafloor topography cause significant variability in tsunami wave heights. For example, the maximum computed wave amplitude at Site 6 (northern coast of Mayne Island) was 12.2 m whereas the maximum height at a nearby station a few kilometres to the south was 18.0 m.

Figure 15 shows that the main areas of possible risk from tsunami waves generated by a delta-front failure off the Fraser River are the central eastern coast of Galiano Island and the northeastern coast of Mayne Island. Maximum computed hypothetical

wave heights for these coasts are 14 to 15 m and 17 to 18 m, respectively. In contrast, the western coast of the Fraser Delta near Tsawwassen is relatively well protected by shallow Roberts Bank, despite the former's proximity to the source region.

5.3 Sensitivity Analysis

Sensitivity tests of the model for the Strait of Georgia are similar to those presented for Malaspina Strait (Subsection 4.3). These tests were made for three selected sites (Fig. 12): Site 4, the northeastern coast of Galiano Island, Site 2, the mid-channel, and Site 3, Point Roberts. Numerical simulations of maximum wave heights span ranges of slide density ($1.6 \leq \rho_2 \leq 2.2$ g $\cdot$ cm^{-3}) and slide kinematic viscosity ($10^{-3} \leq \nu \leq 10^{0}$ m^2 $\cdot$ s^{-1}). Because the inner boundary of the slide is fixed by the position of Roberts Bank, the effects of changing offshore slide position were not relevant to this study. The sensitivity tests were provided for "large" and "small" failure scenarios (Cases 1 and 2) both for high and low water. As an example, Table 5 presents results of computations for Case 1, low water. The results for the other computations were qualitatively similar.

The results of the sensitivity tests for the Strait of Georgia were similar to those for Malaspina Strait, with variations in slide density having a greater effect on computed tsunami heights than variations in kinematic viscosity. However, in

Table 5

Maximum crest and trough heights for three sites in the southern Strait of Georgia computed for various initial viscous slide parameters (Case 1, low water). NA = not applicable

Parameters	Sites					
	4		2		3	
	Crest (m)	Trough (m)	Crest (m)	Trough (m)	Crest (m)	Trough (m)
Slide density (g $\cdot$ cm^{-3})[1]						
1.6	4.3	NA	7.8	−3.6	2.1	−1.7
1.8	5.9	−4.4	9.9	−6.8	2.6	−2.0
1.9	6.7	−4.9	10.9	−10.5	2.8	−1.9
2.0	7.5	−5.0	11.8	−11.2	3.1	−2.5
2.1	8.3	−5.5	12.7	−11.7	3.3	−2.4
2.2	9.1	−5.6	13.7	−12.1	3.5	−2.6
Kinematic viscosity (m^2 $\cdot$ s^{-1})[2]						
0.001	7.9	NA	12.1	NA	3.1	NA
0.01	7.8	NA	12.0	−10.7	3.1	−2.1
0.05	7.5	−5.0	11.8	−11.2	3.1	−2.5
0.1	7.2	−5.4	11.2	−9.8	3.0	−2.2
1.0	5.8	−3.8	10.8	−8.4	2.9	−1.9

[1] Computations are made for different density values for fixed viscosity $\nu = 0.05$ m^2 $\cdot$ s^{-1}.
[2] Computations are made for different viscosity values for fixed slide density $\rho_2 = 2.0$ g $\cdot$ cm^{-3}.

general, the influence of both parameters on tsunami waves for the region of the Strait of Georgia was much greater than for Malaspina Strait. The reason is that the hypothetical slide body used in the Fraser River delta failure was much larger than in the Malaspina case. Resultant nonlinear processes played a much more significant role in the generation of tsunami waves for the Strait of Georgia case. A change in ν from 0.01 to 0.1 caused a change in tsunami amplitude of about 8–11%. For small values of viscosity ($\nu \leq 0.01\ \mathrm{m^2 \cdot s^{-1}}$), numerical stability was a problem and we could not estimate wave heights for certain sites. Variations in slide density ρ_2 of $0.4\ \mathrm{g \cdot cm^{-3}}$ (from 1.6 to $2.0\ \mathrm{g \cdot cm^{-3}}$) resulted in a factor of 1.5–2.5 increase in simulated tsunami amplitudes. Our numerical tests show that computed wave heights for this region are sensitive to the initial slide parameters, so the simulated tsunami heights may be used only as preliminary estimates of the tsunami risk for this coast.

6. Discussion

For any theoretical model applied to natural phenomena, especially when there are no observational data which could be used for direct comparison and verification of the model, it is important to understand clearly the validity of the assumptions used in the model and the limitations inherent in the results. Our model is based on a long-wave (shallow-water) approximation, which is valid for low gradient slopes (for example, JIANG and LEBLOND, 1992, 1994, used this model only for slopes less than 10°). However, actual submarine slopes along the British Columbia coast are often much steeper. In particular, the Texada slope (Malaspina Strait) in the slide source area is approximately 16° (Fig. 4) and the upper delta front of the Fraser River is characterised by slopes of up to 23°. Therefore, we have to estimate the validity of long-wave assumption for such steep slopes.

HEINRICH *et al.* (2000) and ASSIER-RZADKIEWICZ *et al.* (2000) presented the following equation for the force moving a viscous slide down a uniform steep slope:

$$F_\theta = -g\frac{\rho_2 - \rho_1}{\rho_2}\left(\frac{dD_\theta}{dx}\cos\theta - \sin\theta\right) = -g\frac{\rho_2 - \rho_1}{\rho_2}\cos\theta\left(\frac{dD_\theta}{dx} - \tan\theta\right)\ , \qquad (9)$$

where θ is the slope angle, and F_θ is the force of a unit mass in the direction parallel to the slope. In contrast to the models by JIANG and LEBLOND (1992, 1994), this equation considers only the action of the viscous slide on water (''one-way coupling''), but does not take into account the wave resistance, i.e., the influence of surface waves on the slide (''double coupling''). The JLB94 considers full coupling between water waves and slide movement, but assumes a gentle slope. Neglecting the wave influence on the slide, the forcing term in the JBL94 model may be presented as:

$$F_x = -g\frac{\rho_2 - \rho_1}{\rho_2}\left(\frac{dD}{dx} - \tan\theta\right)\ , \qquad (10)$$

where F_x is the force in the horizontal direction. Taking into account that $F_x = F_\theta \cos\theta$, we see that equation (9) differs from equation (10) approximately by the factor $f = \cos^2\theta$. For example, for $\theta = 16^\circ$ (Texada slope) $f = 0.92$, and for $\theta = 23^\circ$ (Fraser River slope) $f = 0.85$. Thus, in the first case, the possible error is about 8%, and in the second case 15%.

Numerical simulation of submarine landslides and associated waves for the two areas considered also provides us an opportunity to examine resonance effects for a natural basin on effectiveness of tsunami wave generation. The coupling between the moving slide and the surface gravity waves it has generated strongly depends on the relative speeds of the wave and the slide. Resonance occurs when the speed of the slide, U, is equal to the local long-wave speed, $c = \sqrt{gh}$, for which the Froude number $Fr = U/c = 1.0$. Here, $h = h(x, y)$ is the water depth under the leading wave. In practice, landslide speed is a function of the slide density, slope angle and the properties of the underlying surface (i.e., the bottom friction coefficient) (PELINOVSKY and POPLAVSKY, 1997) and can be easily estimated numerically. It is incorrect to incorporate artificially predefined slide speeds in models.

In contrast to a rigid-body slide, which moves as an entity with a single speed, different parts of a viscous slide move with different speeds, causing the slide to spread. Following JIANG and LEBLOND (1992), we estimated U_f, the speed of the front, and the associated Froude number, $Fr = U_f/c$. The maximum value of $U_{f_{\max}}$ for Malaspina Strait model is 19.5 m/s (at $\Delta x = 0.90$ km), and the maximum Froude number $Fr_{\max} = 0.46$ (at $\Delta x = 0.85$ km) (Figs. 16a,b). Plots of wave speed c used to estimate Fr for the viscous slide and the corresponding water depth are provided in Figures 16a and 16c, respectively.

For comparison, we also ran several numerical experiments for a rigid slide with different friction coefficients, k ($k = 0$ to 0.20), and compared the results; comparisons were also made with the viscous slide model. Figures 16a,b present slide speeds (U^k) for various friction coefficients and respective Froude numbers ($Fr^k = U^k/c$). Here, the dynamic Coulomb friction coefficient is defined as $k = \tan\psi$, where ψ is the critical incline angle of the depth profile at which a solid block slides without accelerating or decelerating (WATTS, 2000). In the present case, we can specify ψ as a typical incline angle of the eastern Texada slope (i.e., $\psi \approx 6^\circ$), so that $k \approx 0.10$.

For the most realistic case, $k = 0.10$, the maximum slide speed $U^k_{\max} = 33.1$ m/s is achieved at an offshore distance $\Delta x = 1.86$ km, whereas, the maximum Froude number, $Fr_{\max} = 0.61$, occurs at $\Delta x = 0.95$ km; i.e. much closer to shore. The corresponding values for $k = 0.15$ are: $U^k_{\max} = 23.1$ m/s ($\Delta x = 1.21$ km) and $Fr_{\max} = 0.53$ ($\Delta x = 0.83$ km). As indicated by Figure 16, the Froude number quickly reaches a maximum as the slide accelerates downslope, gradually decreasing as the depth increases. The slide stops when the slope diminishes. The run-out distance travelled by the slide, x_s, is highly dependent on the friction coefficient such that $x_s = 5.19, 3.13, 2.29$, and 1.58 km for $k = 0.05, 0.10, 0.15$, and 0.20, respectively. For $k \leq 0.07$, the rigid slide crosses the deepest part of the channel ('thalweg line') and

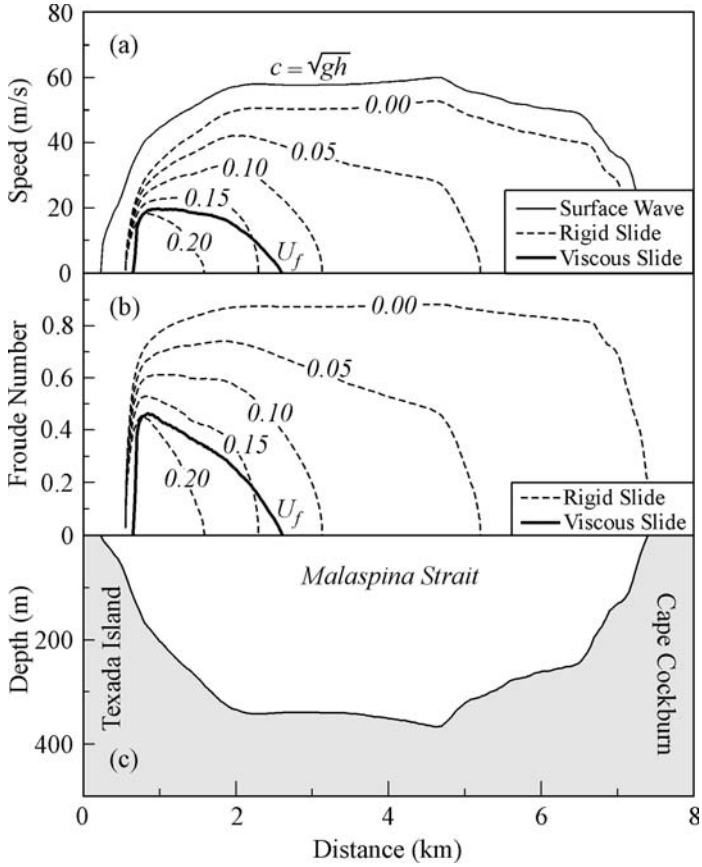

Figure 16
(a) Computed speeds, U, for the rigid-body slide for various friction coefficients ($k = 0$ to 0.20), along with the frontal speed of the viscous slide, U_f. The phase speed of the surface long waves, $c = \sqrt{gh}$, is provided for comparison. (b) The Froude number, $Fr = U/c$, derived from slide body speeds presented in (a). (c) Depth profile across Malaspina Strait in the centre of the computational area.

climbs the opposite slope. The rigid-body slide with $k > 0.15$ has greater speed and Froude number than the viscous slide. However, the viscous slide invariably moves farther downslope ($x_s = 2.60$ km).

In all cases, $U^k < c$, and $Fr^k < 1$ (Fig. 16a). This result follows from the properties of the underwater slide. For the non-friction case ($k = 0$), the slide speed is

$$U^0 = \sqrt{2g'(h_0 - h)} \ , \tag{11}$$

where h_0 is the initial water depth and g' is the reduced gravity,

$$g' = \frac{\rho_2 - \rho_1}{\rho_2} g \ . \tag{12}$$

According to (11) and (12), if $\rho_2 \leq 2.0$ g/cm^3, then $U^0 < c$. For $\rho_2 = 2.0$ g/cm^3, we find $U^0 = c$ when $h_0 = 0$ (i.e., when the slide first begins to move away from the coast). The frictional speeds U^k normally are much less than U^0 (see Fig. 16a). Thus, resonance can occur only if $\rho_2 > 2.0$ g/cm^3 (i.e., for consolidated sediments and rock) or if the slide starts above water. However, even in the latter case, resonance would not hold for very long, since the phase speed of the slide-generated surface waves rapidly increases with water depth and slide body speed is impeded by friction (JIANG and LEBLOND, 1992). We therefore conclude that for submarine slides (for which density $\rho_2 \leq 2.0$ g/cm^3), *resonance coupling of slides and surface waves is physically impossible*.

However, even without resonance coupling, failure of a large accumulation of sediments could produce a destructive landslide-generated tsunami, as the present study demonstrates for the Malaspina Strait and the southern Strait of Georgia. The Fraser River discharges a large mass of sediment which is deposited in the adjacent waters of the Strait of Georgia. Thick deposits of unstable sediments could conceivably become the source of major submarine slides and associated tsunamis in this area as many authors have suggested (cf., TERZAGHI, 1956; MATHEWS and SHEPARD, 1962; TIFFIN *et al*., 1971; HAMILTON and WIGEN, 1987; MCKENNA *et al*., 1992; CHRISTIAN *et al*., 1997a,b, CHILLARIGE *et al.,* 1997a,b). Similar problems presumably apply to other major river deltas along the Pacific Coast of North America. In this context, we note that the simulated wave heights for the southern Strait of Georgia (up to 18 m) are actually even smaller than the observed slide-generated waves that occurred in several deltaic regions of the Alaskan Coast during the 1964 "Good Friday Earthquake," which were higher than 30 m (LANDER, 1996; PALMER, 1999).

For the Fraser River delta we considered large (0.75 km^3), and small (0.23 km^3) hypothetical slide bodies, and found that for this area the simulated tsunami wave heights are approximately proportional to the slide volume. For the large volume slide, computed tsunami heights were a factor of 3 higher than for the small slide.

Comparison of our computations with those of DH93 reveals that tsunami wave heights depend even more on the behaviour of the slide than on the slide volume. The DH93 *retrogressive* slide for the Fraser River delta failure produced much smaller tsunami waves than the *single-body* slide considered in the present study, even though the former was approximately 10 times larger. It is very difficult to say without very thorough geotechnical studies which of these two scenarios is more realistic. The scenario considered in this paper (single-body slide) is the "worst-case scenario."

The sensitivity analysis, presented in Subsection 5.3, demonstrates significant influence of certain slide parameters (slide density and viscosity) on resulting wave heights. However, in general, changes of these parameters, as well as some assumptions made in applying the viscous slide model, play a secondary role in comparison with two major factors: slide volume and initial behaviour of the slide.

7. Conclusions

The viscous slide model used in the present study is an improved and modified version of the three-dimensional numerical model developed by JIANG and LEBLOND (1994). Using this model and available seafloor morphology data, we have examined two zones of potentially unstable sediment deposits: The eastern slope of Texada Island in Malaspina Strait and Roberts Bank on the Fraser River delta-front in the southern Strait of Georgia. Simulated tsunami wave amplitudes for the chosen slide parameters reached 6 to 8 m in the Malaspina Strait region and 18 m in the southern Strait of Georgia region.

While there is insufficient geotechnical information available to know if failure is likely in the two modelled areas of the Strait of Georgia, we have assumed particular scenarios in order to demonstrate the application of state-of-the-art numerical modelling of landslide-generated tsunamis. Considerably more geotechnical data will be required before rigorous assessments of tsunami risk can be undertaken.

7.1. Malaspina Strait

Model results show that a positive semi-wave (wave crest) propagates eastward across the strait toward the mainland coast and a negative semi-wave (wave trough) moves westward toward Texada Island, the latter having the highest amplitudes (4–5 m). On the opposite side of the channel, near Cape Cockburn, modelled wave amplitudes are estimated to reach 1 m. Wave trapping and excitation of shelf seiches are observed on the eastern side of the channel. Periods for the generated tsunami waves range from 10 to 80 s for various sites within the strait. At Site A, periods decrease from 80 to 40 s over time. Our computations demonstrate that the eastern side of Texada Island would be at the highest tsunami risk. Significant waves also are produced on the opposite coast of Malaspina Strait.

The fluid slide spreads out as it moves downslope in Malaspina Strait, attaining a maximum run-out width of about 1 km at the thin leading edge of the slide, about 2.5 km from the coast (Fig. 7). Unlike a rigid slide, which terminates at a single location, the fluid slide is distributed unevenly down the slope. The slide has a fan-like (arcuate) shape with the axis of the slide consisting of two central lobes of thicker material. The maximum speed attained by the leading edge of the viscous slide, $U_{f_{\max}} \approx 19$ m/s, based on the assumed input parameters used for this modelling, is achieved at an offshore distance of about 0.9 km. At all times, the slide speed is markedly less than the phase speed $c = \sqrt{gh}$ of the long surface waves so that the Froude number, $Fr = U_f/c < 1.0$. Simple theoretical estimates show that if the slide density $\rho_2 \leq 2.0$ g/cm^3 (typical values of sediment density are 1.2–2.0 g/cm^3), then $U < c$ and resonant coupling of slides and surface waves is physically impossible.

7.2. Southern Strait of Georgia

We considered two hypothetical deep-seated failure scenarios of Fraser River delta-front sediments, both occurring at a depth of about 100 m: (a) A large, 7×3 km^2 (0.75 km^3), failure; and (b) a small, 4×2.6 km^2 (0.23 km^3) failure. Both failures were assumed to be purely submarine and were modelled for both extreme high-tide and extreme low-tide conditions. The main results of our simulation of tsunami waves in the southern Strait of Georgia caused by these failures are:

1. Extreme wave crests of 2 to 18 m are generated by the large (Case 1) delta failure while wave crests of 0.8 to 8.5 m are generated by the small (Case 2) delta failure. Maximum simulated wave amplitudes occur on the southwest side of the strait, opposite the source area, with amplitudes of 14 to 15 m on the coast of Galiano Island and 18 m on the coast of Mayne Island. Amplitudes on the eastern side of the strait near the Tsawwassen Ferry Terminal and Fraser River delta are much smaller (1 to 4 and 0.2 to 2 m, respectively) because of the efficient wave reflection at the outer edge of Roberts Bank.

2. The leading semi-wave from the landslides consists of a positive wave propagating into the deep portion of the basin toward the southwest. The first trough, which would normally propagate onshore, is immediately reflected back into the strait by Roberts Bank. For slides occurring close to the bank, the most destructive waves are those reflected from the opposite side of the strait. These waves can penetrate into shallow water and inundate the mainland coast. Significant nonlinear effects can be expected in this case. The slide body moving downslope on the Fraser Delta could reach speeds of about 20 m/s.

3. Comparison of ''low-tide'' and ''high-tide'' numerical simulations indicates that simulated waves are 5–10% higher at low tide, apparently because the slide body is located closer to the sea surface. However, because water levels are 6 m higher at high tide than low tide, the destructive capacity of the tsunami waves at the coast is greater during high tide.

Acknowledgements

This research was partially sponsored by BC Hydro through a joint agreement with the Geological Survey of Canada, Pacific Geoscience Centre and by INTAS project 99–1600. Swath bathymetric data were provided by the Pacific Geoscience Centre. We wish to thank Hal Mofjeld for his very productive comments, Fred Stephenson for encouragement throughout this study, Ralph Currie and David Mosher for their assistance with the geomorphic data, and Patricia Kimber for drafting the figures. The reviewer, Don Dunbar, provided helpful comments and suggestions on many aspects of this work.

References

Altinok, Y., Alpar, B., Ersoy, S., and Yalciner, A. C. (1999), *Tsunami Generation of the Kocaeli Earthquake (August 17th, 1999) in the Izmit Bay: Coastal Observations, Bathymetry and Seismic Data*, Turkish J. Marine Sciences *5 (3)*, 131–148.

Andresen, A. and Bjerrum, L. (1967), *Slides in subaqueous slopes in loose sand and silt*. In *Marine Geotechnique* (ed. Richards A. F.) (Univ. Illinois Press, Urbana), pp. 221–239.

Assier-Rzadkiewicz, S., Mariotti, C., and Heinrich, P. (1997), *Numerical Simulation of Submarine Landslides and their Hydraulic Effects*, J. Waterways, Port, Coastal and Ocean Eng., ASCE *123 (4)*, 149–157.

Assier-Rzadkiewicz, S., Heinrich, P., Sabatier, P. C., Savoye, B., and Bourillet, J. F. (2000), *Numerical Modelling of Landslide-generated Tsunami: The 1979 Nice Event*, Pure Appl. Geophys. *157*, 1707–1727.

Bernard, E. N. (1998), *Program Aims to Reduce Impact of Tsunamis on Pacific States*, Earth in Space *11 (2)*, 1–16.

Bjerrum, L. (1971), *Sub-aqueous Slope Failures in Norwegian Fjords*, Publ. 88, Norw. Geotech. Inst., Oslo, 8 p.

Chillarige, A.V., Robertson, P. K., Morgenstern, N. R., and Christian, H. A. (1997a), *Evaluation of the In Situ State of Fraser River Sand*, Can. Geotech. J. *34*, 510–519.

Chillarige, A. V., Morgenstern, N. R., Robertson, P. K., and Christian, H. A. (1997b), *Seabed Instability due to Flow Liquefaction in the Fraser River Delta*, Can. Geotech. J. *34*, 520–533.

Christian, H. A., Barrie, J. V., Hunter, J. A., Luternauer, J. L., and Monahan, P. A. (1995), *Deep Hole Geotechnical Investigation, Westshore Terminal, Roberts Bank Superport*, March 6–31, 1995, Open File Report, Geological Survey of Canada, pp 30.

Christian, H. A., Woeller, D. J., Robertson, P. K., and Courtney R. C. (1997a), *Site Investigations to Evaluate Flow Liquefaction Slides at Sand Heads, Fraser River Delta*, Can. Geotech. J. *34*, 384–397.

Christian, H. A., Mosher, D. C., Mulder, T., Barrie, J. V., and Courtney, R. C. (1997b), *Geomorphology and Potential Slope Instability on Fraser River Delta Foreslope, Vancouver, British Columbia*, Can. Geotech. J. *34*, 432–446.

Clague, J. J. (2001), *Tsunamis*. In *A Synthesis of Geological Hazards in Canada* (ed. Brooks, G. R.), Geological Survey of Canada, Bull. *548*, 27–42.

Cornforth, D. H. and Lowell, J. A. (1996), *The 1994 submarine slope failure at skagway, Alaska*. In *Landslides* (Balkema, Rotterdam, 1996), pp. 527–532.

Currie, R. G. and Mosher, D. C. (1996), *Swath Bathymetric surveys in the Strait of Georgia, British Columbia*. In *Current Research*, *Part E*, Geological Survey of Canada, 33–40.

Dunbar, D. S. and Harper, J. R. (1993), *Numerical Simulation of Tsunamigenic Submarine Slope Failure in the Fraser River Delta, British Columbia*, Marine Geodesy *16*, 101–108.

Dunbar, D. S., LeBlond, P. H., and Murty, T. S. (1991), *Evaluation of Tsunami Amplitudes for the Pacific Coast of Canada,* Prog Oceanog *26,* 115–177.

Evans, S. G. (2001), *Landslides*. In *A Synthesis of Geological Hazards in Canada* (ed. Brooks, G. R.), Geological Survey of Canada, Bull. *548*, 43–79.

Fine, I. V., Rabinovich, A. B., Kulikov, E. A., Thomson, R. E., and Bornhold, B. D. (1998), *Numerical Modelling of Landslide-Generated Tsunamis with Application to the Skagway Harbor Tsunami of November 3, 1994*. In *Proceedings, International Conference on Tsunamis* (Paris, 1998) pp. 211–223.

Go, C. N., Kaistrenko, V. M., and Simonov, K. V. (1985), *A Two-Parameter Scheme for Tsunami Hazard Zoning*, Marine Geodesy *9*, 469–476.

Hamilton, T. S. and Luternauer, J. L. (1983), *Evidence of Sea Floor Instability in the Southcentral Strait of Georgia, British Columbia: A Preliminary Compilation*, Geological Survey of Canada, Pap. *83–1A*, 417–421.

Hamilton, T. S. and Wigen, S. O. (1987), *The Foreslope Hills of the Fraser River Delta: Implication of Tsunamis in Georgia Strait*, Science of Tsunami Hazards *5*, 15–33.

Harbitz, C. B. (1992), *Model Simulations of Tsunamis Generated by the Storegga Slides*, Marine Geology *105*, 1–21.

HEBENSTREIT, G. T. and MURTY, T. S. (1989), *Tsunami Amplitudes from Local Earthquakes in the Pacific Northwest Region of North America, Part 1, The Outer Coast*, Marine Geodesy *13,* 101–146.

HEINRICH, P. (1992), *Nonlinear Water Waves Generated by Submarine and Aerial Landslides*, J. Waterways, Port, Coastal and Ocean Eng., ASCE *118 (3)*, 249–266.

HEINRICH, P., MANGENEY, A., GUIBOURG, S., ROCHE, R., BOUDON, G., and VHEMINÉE, J.-L. (1998), *Simulation of Water Waves Generated by a Potential Debris Avalanche in Montserrat, Lesser Antilles*, Geophys. Res. Lett. *25 (19)*, 3697–3700.

HEINRICH, P., PIATENSI, A., OKAL, E., and HÉBERT, H. (2000), *Near-field Modeling of the July 17, 1998 Tsunami in Papua New Guinea*, Geophys. Res. Lett. *27*, 3037–3040.

IMAMURA, F. (1996), *Review of Tsunami Simulation with Finite Difference Method*. In *Long-Wave Runup Models* (eds. Yeh, H., Liu, P., and Synolakis, C.) (World Scientific, London, 1996), pp. 25–42.

IMAMURA, F. and GICA, E. C. (1996), *Numerical Model for Tsunami Generation due to Subaqueous Landslide Along a Coast*, Science of Tsunami Hazards *14 (1)*, 13–28.

IMAMURA, F., HASHI, K., and IMTEAZ, Md. M. A. (2001), *Modeling for tsunamis genarated by landsliding and debris flow*. In *Tsunami Research at the End of a Critical Decade* (ed. Hebenstreit, G.) (Kluwer, Dorderecht, 2001, 209–228).

IWASAKI, S. I., FURUMOTO, A., and HONZA, E. (1996), *Can be a Submarine Landslide be Considered as a Tsunami Source?* Science of Tsunami Hazards *14 (2)*, 89–100.

JANSEN, E., BEFRING, S., BUGGE, T., EIDVIN, T., HOLTEDAHL, H., and SEJRUP, H.-P. (1987), *Large Submarine Slides on the Norwegian Continental Margin: Sediments, Transport, and Timing*, Marine Geology *78*, 77–107.

JIANG, L. and LEBLOND, P. H. (1992), *The Coupling of a Submarine Slide and the Surface Waves which it Generates*, J. Geophys. Res. *97 (C8)*, 12,731–12,744.

JIANG, L. and LEBLOND, P. H. (1994), *Three-Dimensional Modeling of Tsunami Generation due to a Submarine Mudslide*, J. Phys. Oceanogr. *24 (3)*, 559–572.

JOHNS, M. W., PRIOR, D. B., BORNHOLD, B. D., COLEMAN, J. M., and BRYANT, W. R. (1986), *Geotechnical Aspects of a Submarine Slope Failure, Kitimat Fjord, British Columbia*, Marine Geotechnology 6, 243–279.

JOHNSON, A. M. (1970), *Physical Process in Geology* (Freeman, San Francisco), pp. 557.

KANAMORI, H. (1972), *Mechanism of Tsunami Earthquakes*, Phys. Earth Planet Inter *6*, 346–359.

KARLSRUD, K. and EDGERS, L. (1980), *Some aspects of submarine slope stability*. In *Marine Slides and Other Mass Movements* (Plenum, New York, 1980), pp. 61–81.

KOWALIK, Z. (1997), *Landslide-generated Tsunami in Skagway, Alaska*, Science of Tsunami Hazards *15 (2)*, 89–106.

KULIKOV, E. A., RABINOVICH, A. B., THOMSON, R. E., and BORNHOLD, B. D. (1996), *The Landslide Tsunami of November 3, 1994, Skagway Harbor, Alaska*, J. Geophys. Res. *101 (C3)*, 6609–6615.

KULIKOV, E. A., RABINOVICH, A. B., FINE, I.V., BORNHOLD, B. D., and THOMSON, R. E. (1998), *Tsunami Generation by Landslides at the Pacific Coast of North America and the Role of Tides*, Oceanology *38 (3)*, 323–328.

LANDER, J. F. (1996), *Tsunamis Affecting Alaska, 1737–1996* (Boulder, U. S. Dep. Comm., 1996), pp. 195.

LUTERNAUER, J. L. and FINN, W. D. L. (1983), *Stability of the Fraser River Delta Front*, Can. Geotech. J. *20*, 603–616.

MATHEWS, W. A. and SHEPARD, E. P. (1962), *Sedimentation of the Fraser River Delta, British Columbia*, Bull. Amer. Assoc. Petr. Geologists *46*, 1416–1438.

MCKENNA, G. T. and LUTERNAUER, J. L. (1987), *First Documented Large Failure at the Fraser River Delta Front, British Columbia*, Geological Survey of Canada, Pap. *87-1A*, 919–924.

MCKENNA, G. T., LUTERNAUER, J. L., and KOSTASCHUK, R. A. (1992), *Large-scale Mass-wasting Events on the Fraser River Delta near Sand Heads, British Columbia*, Can. Geotech. J. *29*, 151–156.

MILLER, D. J. (1960), *The Alaska Earthquake on July 10, 1958: Giant Wave in Lituya Bay*, Bull. Seismoc. Soc. Am. *50 (2)*, 253–266.

MILOH, T. and STRIEM, H. L. (1978), *Tsunami Effects at Coast Sites due to Offshore Faulting*, Technophysics *46*, 347–356.

MOFJELD, H. O., GONZÁLEZ, F. I., and NEWMAN, J. C. (1999), *Tsunami prediction in U.S. coastal regions*. In *Coastal Ocean Prediction, Ch. 14, Coastal and Estuarine Studies 56* (ed. Mooers, C. N. K.), AGU, pp. 353–375.

MURTY, T. S. (1977), *Seismic Sea Waves – Tsunamis*. Bull. Fish. Res. Board Canada 198, Ottawa, pp. 337.

MURTY, T. S. (1979), *Submarine Slide-generated Water Waves in Kitimat Inlet, British Columbia,* J. Geophys. Res. *84 (C12)*, 7777–7779.

MURTY, T. S. and HEBENSTREIT, G. T. (1989), *Tsunami Amplitudes from Local Earthquakes in the Pacific Northwest Region of North America, Part 2, Strait of Georgia, Juan de Fuca Strait, and Puget Sound*, Marine Geodesy *13,* 189–209.

NG, M., LEBLOND, P. H., and MURTY, T. S. (1990), *Numerical Simulation of Tsunami Amplitudes on the Coast of British Columbia due to Local Earthquakes*, Marine Geodesy *13,* 101–146.

PALMER, S. (1999), *Geotechnical Considerations for the Proposed Southwest Harbor CAD Facility*, Unpublished Manuscriot, DNR Geology Division, pp. 42.

PELINOVSKY, E. and POPLAVSKY, A. (1996), *Simplified Model of Tsunami Generation by Submarine Landslides*, Phys. Chem. Earth *21 (12)*, 13–17.

Planning for Risk: Comprehensive Planning for Tsunami Hazard Areas (1988), Prepared by Urban Regional Research for the National Science Foundation, pp. 246.

PRIOR, D. B., WISEMAN, W. J., and BRYANT, W. R. (1981), *Submarine Chutes on the Slopes of Fjord Deltas*, Nature *290*, 5804, 326–328.

PRIOR, D. B., BORNHOLD, B. D., and JOHNS, M. W. (1984), *Depositional Characteristics of a Submarine Debris Flow*, J. Geology *92*, 707–727.

RABINOVICH, A. B. and SHEVCHENKO, G. V. (1990), *Estimation of extreme sea level heights as the superposition of tides, storm surges and tsunamis*. In *Proc. IUGG/IOC Intern. Tsunami Symp.* (Novosibirsk, 1989), pp.. 201–206.

RABINOVICH, A. B., THOMSON, R. E., KULIKOV, E. A., BORNHOLD, B. D., and FINE, I.V. (1999), *The Landslide-generated Tsunami of November 3, 1994 in Skagway Harbor, Alaska: A Case Study*, Geophys. Res. Lett. *26 (19)*, 3009–3012.

REN, P., BORNHOLD, B. D., and PRIOR, D. B. (1996), *Seafloor Morphology and Sedimentary Processes, Knight Inlet, British Columbia*, Sedimentary Geology *103*, 201–228.

ROACHE, P. J. *Computational Fluid Dynamics* (Hermousa Publ., Albuquerque, N. M. 1976), pp. 446.

ROGERS, G. C. (1980), *A Documentation of Soil Failure during the British Columbia Earthquake of 23 June, 1946*, Can. Geotech. J. *17*, 122–127.

ROGERS, G. C. and HASEGAWA, H. S. (1978), *A Second Look at the British Columbia Earthquake of 23 June, 1946*, Bull. Seismol. Soc. Am. *68 (3)*, 653–675.

SILVIS, F. and DE GROOT, M. B. (1995), *Flow Slides in the Netherlands: Experience and Engineering Practice*, Can. Geotech. J. *32*, 1086–1092.

SIMPSON, J. E., *Gravity Currents: In the Environment and the Laboratory* (Halsted Press, England, 1987), pp. 244.

SLADEN, J. A., D'HOLLANDER, R. D., KRAHN, J., and MITCHELL, D. E. (1985), *Back Analysis of the Nerlerk Berm Liquefaction Slides*, Can. Geotech. J. *22*, 579–588.

SOLOVIEV, S. L. and GO, CH. N. (1975), *Catalogue of Tsunamis on the Eastern Shore of the Pacific Ocean* (Nauka Publ. House, Moscow, 1975), pp. 204. (in Russian; English translation: Canadian Transl. Fish. Aquatic Sci., No. 5078, Ottawa, 1984, pp. 285.).

TAPPIN, D. *et al.* (1998), *Sediment Slump Likely Caused 1998 Papua New Guinea Tsunami*, EOS *80*, 329, 334, 340.

TERZAGHI, K. (1956), *Varieties of submarine slope failures*. In *8th Texas Conference on Soil Mechanics and Foundation Engineering* (Houston, Harvard Soil Mech. Comm., 1956), pp. 41.

THOMSON, R. E. (1981), *Oceanography of the British Columbia Coast,* (Canadian Spec. Publ. Fish. Aquat. Sci. 56, Ottawa), pp. 291.

THOMSON, R. E., RABINOVICH, A. B., KULIKOV, E. A., FINE, I.V., and BORNHOLD, B. D. (2001), *On numerical simulation of the landslide-generated tsunami of November 3, 1994 in Skagway Harbor, Alaska*. In *Tsunami Research at the End of a Critical Decade* (ed. Hebenstreit G.) (Kluwer, Dorderecht, 2001) 243–282.

TIFFIN, D. L., MURRAY, J. W., MYERS, I. R., and GARRISON, R. E. (1971), *Structure and Origin of the Foreslope Hills, Fraser Delta, British Columbia*, Bull. Can. Petr. Geol. *19*, 589–600.

TITOV, V. and GONZÁLEZ, F. (2001), *Numerical study of the source of the July 17, 1998 PNG tsunami*. In *Tsunami Mitigation* (ed. Hebenstreit G.) (Kluwer, Dorderecht, 2001) (in press).

WATTS, P. (2000), *Tsunami Features of Solid Block Underwater Landslides*, J. Waterways, Port, Coastal and Ocean Eng., ASCE *126 (3)*, 144–152.

WIEGEL, R. L., NODA, E. K., KUBA, E. M., GEE, D. M., and TORNBERG, G. F. (1970), *Water Waves Generated by Landslides in Reservoirs*, J. Waterways, Harbors Coastal Eng., ASCE *96*, 307–333.

(Received March 7, 2001, accepted October 22, 2001)